Mikada, H., Moore, G.F., Taira, A., Becker, K., Moore, J.C., and Klaus, A. (Eds.)
Proceedings of the Ocean Drilling Program, Scientific Results Volume 190/196

4. Composition and Sources of Clay from the Trench Slope and Shallow Accretionary Prism of Nankai Trough[1]

Michael B. Underwood[2] and Joan F. Steurer[2]

ABSTRACT

Three sites were cored on the landward slope of the Nankai margin of southwest Japan during Leg 190 of the Ocean Drilling Program. Sites 1175 and 1176 are located in a trench-slope basin that was constructed during the early Pleistocene (~1 Ma) by frontal offscraping of coarse-grained trench-wedge deposits. Rapid uplift elevated the substrate above the calcite compensation depth and rerouted a transverse canyon-channel system that had delivered most of the trench sediment during the late Pliocene (1.06–1.95 Ma). The basin's depth is now ~3000 to 3020 m below sea level. Clay-sized detritus (<2 µm) did not change significantly in composition during the transition from trench-floor to slope-basin environment. Relative mineral abundances for the two slope-basin sites average 36–37 wt% illite, 25 wt% smectite, 22–24 wt% chlorite, and 15–16 wt% quartz. Site 1178 is located higher up the landward slope at a water depth of 1741 m, ~70 km from the present-day deformation front. There is a pronounced discontinuity ~200 m below seafloor between muddy slope-apron deposits (Quaternary–late Miocene) and sandier trench-wedge deposits (late Miocene; 6.8–9.63 Ma). Clay minerals change downsection from an illite-chlorite assemblage (similar to Sites 1175 and 1176) to one that contains substantial amounts of smectite (average = 45 wt% of the clay-sized fraction; maximum = 76 wt%). Mixing in the water column homogenizes fine-grained suspended sediment eroded from the Izu-Bonin volcanic arc, the Izu-Honshu collision zone, and the Outer Zone of Kyushu and

[1]Underwood, M.B., and Steurer, J.F., 2003. Composition and sources of clay from the trench slope and shallow accretionary prism of Nankai Trough. *In* Mikada, H., Moore, G.F., Taira, A., Becker, K., Moore, J.C., and Klaus, A. (Eds.), *Proc. ODP, Sci. Results,* 190/196, 1–28 [Online]. Available from World Wide Web: <http://www-odp.tamu.edu/publications/190196SR/VOLUME/CHAPTERS/206.PDF>. [Cited YYYY-MM-DD]
[2]Department of Geological Sciences, University of Missouri, Columbia, 101 Geology Building, Columbia MO 65211, USA. Correspondence author: **underwoodm@missouri.edu**

Initial receipt: 15 November 2002
Acceptance: 5 August 2003
Web publication: 26 November 2003
Ms 190SR-206

Shikoku, but the spatial balance among those contributors has shifted through time. Closure of the Central America Seaway at ~3 Ma was particularly important because it triggered intensification of the Kuroshio Current. With stronger and deeper flow of surface water toward the northeast, the flux of smectite from the Izu-Bonin volcanic arc was dampened and more detrital illite and chlorite were transported into the Shikoku-Nankai system from the Outer Zone of Japan.

INTRODUCTION

Trench-slope basins and slope aprons are characteristic of all types of subduction margins (Moore and Karig, 1976a; Scholl et al., 1980; Underwood and Moore, 1995). These dynamic environments are difficult to stereotype, however, because each must adjust to site-specific interplays between subduction-driven deformation and sedimentation. Most slope aprons are fine grained because deposition occurs via slow hemipelagic settling. In theory, strata in flat-floored intraslope basins should be thicker and sandier than those on the inclined slope apron. Direct connections from a juvenile slope basin to the shoreline through submarine canyons or channels are rare, so initial accumulations consist mostly of hemipelagic mud, lutite turbidites, and locally generated slides and mud flows (Underwood and Bachman, 1982). Terrigenous influx should increase with time in response to uplift of the accretionary prism and canyon erosion.

Leg 190 of the Ocean Drilling Program (ODP) provided a rare opportunity to document the early stages of stratigraphic evolution of a trench-slope basin in the Nankai subduction system of southwest Japan (Moore et al., 2001b; Underwood et al., 2003). The basin–prism transition was cored at two sites (Holes 1175A and 1176A) where the accreted strata are Pliocene–early Pleistocene in age (Fig. F1). A third site (1178) was drilled farther upslope where a 200-m-thick slope apron overlies accreted strata of late Miocene age (Fig. F1). The purpose of this paper is to show how clay mineral assemblages and suspended sediment dispersal patterns changed during 10 m.y. of evolution of the Nankai accretionary prism and slope cover.

F1. Bathymetric map of Nankai Trough and Shikoku Basin area, p. 17.

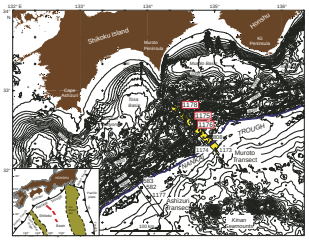

DRILLING RESULTS

Regional Sedimentary and Tectonic Context

The most recent phase of Nankai accretion began ~6 m.y. ago with acceleration of subduction of the Philippine Sea plate (Itoh and Nagasaki, 1996; Kamata and Kodama, 1999). Water depths along the present-day axis of Nankai Trough are <5000 meters below sea level (mbsl), and the axial gradient dips gently to the southwest (Fig. F1). Rates of sediment delivery to the trench were high because of rapid uplift and erosion of the principal detrital source: the collision zone between the Honshu arc and the Izu-Bonin arc (Taira and Niitsuma, 1986; Marsaglia et al., 1992; Underwood et al., 1993). The largest throughgoing sediment conduit, Suruga Trough, extends from the shoreline on the west side of the Izu Peninsula and continues along the northern flank of Zenisu Ridge into the northeast end of the Nankai Trough (Le Pichon et al., 1987b; Nakamura et al., 1987; Soh et al., 1995). The Nankai deep-sea channel meanders from Suruga Trough down the axis of

Nankai Trough to a termination point offshore from the Kii Peninsula (Shimamura, 1989). Fan-shaped sediment mounds are present at the mouths of Tenryu and Shiono-misaki Canyons (Soh et al., 1991), and several smaller canyons probably reach the trench farther to the southwest (Taira and Ashi, 1993). The trench wedge in most places is 450–700 m thick, and the facies pattern thickens and coarsens upward (Moore and Karig, 1976b; Coulbourn, 1986; Taira et al., 1992).

The physiography of the Nankai margin is complicated. Prominent forearc basins on the upper slope (e.g., Muroto, Tosa, and Kumano Basins) intercept sediment emanating from small canyons and slope gullies (Blum and Okamura, 1992). A fault-controlled ridge and trough landscape varies markedly along strike (Le Pichon et al. 1987a, 1987b; Moore et al., 1991; Ashi and Taira, 1992; Morgan et al., 1994; Okino and Kato, 1995). The Muroto segment of the margin (Fig. F1) comprises four structural divisions (Fig. F2) (Moore et al., 2001a). Starting at the prism toe, the imbricate thrust zone is characterized by packages of seaward-vergent thrust faults, with the frontal thrust forming its seaward edge. Out-of-sequence thrusts begin ~20 km landward of the deformation front. The lowermost slope basin of Muroto formed behind the frontal out-of-sequence thrust (Fig. F2). The large thrust-slice zone contains faults that separate previously imbricated packages of relatively coherent strata; strong reflectors are evident beneath the large thrust slices. Hole 1175A penetrated a slope basin in this zone just landward of a major out-of-sequence thrust, at a water depth of 3012.8 mbsl (Fig. F2). Hole 1176A drilled through a separate fault slice at the seaward edge of the same basin at a depth of 3016.8 mbsl (Fig. F2). Farther upslope, the fourth structural zone of Muroto displays high-amplitude semicontinuous reflectors that dip landward beneath a relatively coherent apron of slope sediments. Drilling at Site 1178 (Fig. F2) started at 1716.5 mbsl and penetrated 450 m beneath the slope apron into the landward-dipping reflectors.

F2. Zones of seismic reflection in the Muroto Transect area, p. 18.

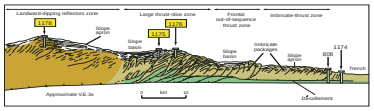

Lithostratigraphy of the Slope Basin

Strata at Sites 1175 and 1176 are grouped into three lithostratigraphic units: upper slope basin, lower slope basin, and slope–prism transition (Fig. F3). The upper slope-basin deposits are Quaternary in age and extend from the seafloor to 224.75 meters below seafloor (mbsf) (Site 1175) and 195.79 mbsf (Site 1176). Hemipelagic mud with abundant calcareous nannofossils is the most common lithology, with local beds and laminae of volcanic ash, sand, clayey sand, and silt. Contorted stratification is another noteworthy aspect of this unit, particularly at Site 1175 (Shipboard Scientific Party, 2001c, 2001d). The lower slope-basin facies is also Quaternary in age and extends from 224.75 to 301.64 mbsf at Site 1175 and from 195.79 to 223.54 mbsf at Site 1176 (Fig. F3). Lithification is more advanced in this unit, and soft-sediment deformation is absent. Poorly sorted and structureless sandy mudstone is the distinguishing lithology; other lithologies include nannofossil-bearing hemipelagic mudstone, volcanic ash, and fine sand. The transition from slope basin to accretionary prism occurs in strata that range from Quaternary to Pliocene in age. Precise identification of the boundary remains elusive (Underwood et al., 2003), but the accreted sediments include carbonate-poor hemipelagic mudstone, poorly indurated silt and sand turbidites, muddy gravel, and pebbly mud (Fig. F3). A polymictic population of pebbles includes abundant quartz, chert, fine-grained sedimentary to meta-sedimentary lithic fragments, and minor

F3. Lithostratigraphic and biostratigraphic correlation, p. 19.

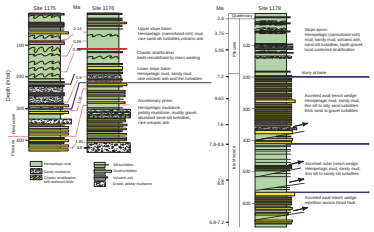

fragments of mafic volcanic rock (Shipboard Scientific Party, 2001c, 2001d). Calcareous nannofossils provide datums for correlation between the two slope-basin sites (Fig. F3). The Pliocene/Pleistocene boundary (1.8 Ma), for example, is located at a depth of 389.27 mbsf in Hole 1175A and 291.63 mbsf in Hole 1176A (Fig. F3). Strata at Site 1176 extend to Zone NN15 (3.8 Ma).

Lithostratigraphy of the Upper Accretionary Prism

The principal drilling objective for Site 1178 was to sample the domain of landward-dipping reflectors as a record of early accretionary prism evolution. Overall, the sedimentary section spans the time interval from late Miocene (6.8–9.63 Ma) through Pleistocene (Subzone NN21a). The slope apron predominantly consists of nannofossil-rich hemipelagic mud, with lesser amounts of sandy mud, silty sand, mud-supported gravel, and volcanic ash. There are also intervals of slump folds and sedimentary brecciation caused by large-scale gravitational failure (Shipboard Scientific Party, 2001e). Seismic reflectors change their orientation to landward dipping below 199.20 mbsf, where poorly lithified turbidites display such deformation features as incipient cleavage, spaced fractures, bedding-oblique foliation, bedding-parallel fissility, and brecciation. The preponderance of sand is consistent with trench-wedge deposition. Scaly surfaces with downdip slickenlines indicate that a major thrust fault is present at 506 mbsf. Faults also create steeper dips and increased deformation at ~550 and 633 mbsf (Fig. F3), and there is an inversion of lithofacies (outer trench wedge over axial trench wedge) at 563.95 mbsf.

METHODS AND MATERIALS

The core intervals that we analyzed from Sites 1175, 1176, and 1178 are listed in Table T1. Shipboard analyses of random bulk powders followed the methods of Shipboard Scientific Party (2001a). **Underwood et al.** (this volume) described sample preparation and X-ray diffraction (XRD) methodology for clay-sized fractions. Briefly, specimens of mud and mudstones were disaggregated in H_2O_2 and sodium hexametaphosphate solution, washed twice by centrifugation, separated into <2-µm size fractions, and transferred as oriented aggregates onto glass slides using the filter-peel method. The clay aggregates were air-dried then saturated in ethylene glycol vapor. The samples were scanned by XRD from 2° to 23°2θ at the following instrument settings: voltage = 40 kV, current = 30 mA, scan rate = 1°2θ/min, step size = 0.01, slits = 0.2 mm. Digital data were processed using MacDiff software to obtain a baseline, smooth counts, correct peak positions (relative to the quartz peak at 20.95°2θ), and calculate peak intensities and areas. Values of relative mineral abundance, expressed as a weight percent of the clay-sized fraction (where smectite + illite + chlorite + quartz = 100%), are based on peak areas for basal reflections (Fig. F4) and a new set of normalization factors that were calculated by matrix singular value decomposition (SVD) (Fisher and Underwood, 1995; **Underwood et al.,** this volume). Small amounts of kaolinite probably contribute to the peak at ~7 Å (Underwood et al., 1993), so we report those values as chlorite (+ kaolinite). To estimate the amount of each clay mineral in bulk mudstone, we multiplied the abundance of total clay minerals (using shipboard data from the nearest bulk powder sample interval) by the weight percent of

T1. X-ray diffraction analyses, p. 26.

F4. Examples of X-ray diffractograms, p. 20.

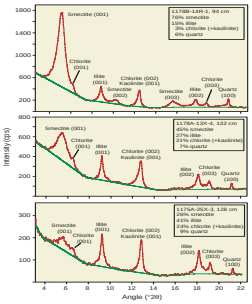

each clay in the <2-µm clay mineral fraction (where smectite + illite + chlorite = 100%). Although bulk powder XRD methods are imperfect, thorough analysis of error shows that the SVD method is accurate to ±5 wt% for standard mineral mixtures (Shipboard Scientific Party, 2001e; **Underwood et al.,** this volume). For comparative purposes, Table **T1** also includes values of relative abundance (weighted peak area percent) using Biscaye (1965) weighting factors.

RESULTS

Slope Basin Sites

Shipboard analyses showed that the content of total clay minerals in bulk powders from Sites 1175 and 1176 does not change appreciably from the slope-basin facies to the accretionary prism (Fig. **F5**). The average total clay mineral content is ~40 wt% relative to quartz, plagioclase, and calcite (Shipboard Scientific Party, 2001c, 2001d). The calcite content of nannofossil-bearing hemipelagic sediments in the slope basin is typically between 15 and 40 wt%; thus, deposition occurred above the calcite compensation depth (CCD). Samples from the underlying accretionary prism contain amounts of total clay minerals similar to those from the slope basin, but the calcite content drops sharply (Fig. **F5**). This depletion of calcite can be explained by poor preservation of calcareous nannofossils below the CCD.

X-ray diffraction results show modest variations in clay mineralogy with depth at both slope-basin sites (Fig. **F6**). The most abundant mineral in the clay-sized fraction is illite. At Site 1175, elative percentages in the slope-basin deposits average 37 wt% illite, 25 wt% smectite, 22 wt% chlorite (+ kaolinite), and 16 wt% quartz (Table **T1**). Slope-basin deposits at Site 1176 are similar in composition, averaging 36 wt% illite, 25 wt% smectite, 24 wt% chlorite (+ kaolinite), and 16 wt% quartz (Table **T1**). We see no statistically meaningful changes in clay mineral content between sites or across the transition from slope basin to accretionary prism (Fig. **F6**). The prism mudstones at Site 1175 average 32 wt% illite, 32 wt% smectite, 25 wt% chlorite (+ kaolinite), and 11 wt% quartz, whereas those at Site 1176 average 31 wt% illite, 29 wt% smectite, 26 wt% chlorite (+ kaolinite), and 14 wt% quartz. Percentages of smectite in the bulk mud are generally <15 wt% (Table **T1**).

Slope Apron Site

Shipboard data from Site 1178 show that the total clay-mineral content increases toward the base of the slope apron (Fig. **F5**). Total clay at the top of the section is ~26 wt% (relative to quartz, plagioclase, and calcite), but values increase steadily to 48 wt% at 156 mbsf (Shipboard Scientific Party, 2001d). The calcite content of hemipelagic sediments in the slope basins decreases from 43 to 1 wt% over the same depth interval. Samples from the underlying accretionary prism are nearly devoid of calcite, and total clay minerals vary between 31 and 58 wt% (Fig. **F5**).

Compared to slope-basin sites, the slope-apron facies at Site 1178 shows more scatter in relative clay mineral abundances (Fig. **F7**). More significant is the substantial increase in the amount of expandable clay minerals (20–62 wt%). Mudstones in the underlying accretionary prism average 45 wt% smectite, 26 wt% illite, 20 wt% chlorite (+ kaolinite),

F5. Calcite and total clay minerals in bulk samples, p. 21.

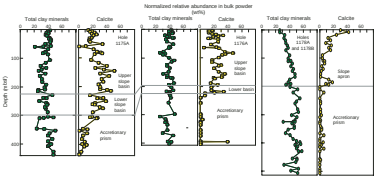

F6. Smectite, illite, chlorite (+ kaolinite), and quartz in mud and mudstone, Sites 1175 and 1176, p. 22.

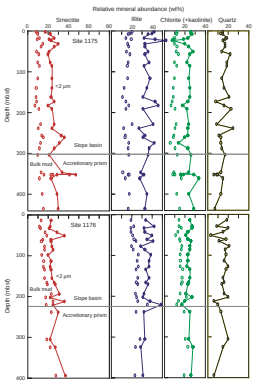

F7. Smectite, illite, chlorite (+ kaolinite), and quartz in mud and mudstone, Site 1178, p. 23.

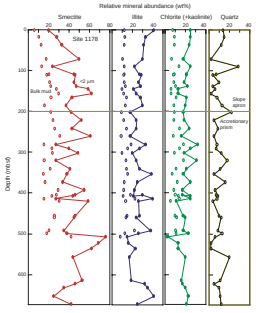

and 9 wt% quartz (Table T1). The highest value for smectite in the clay fraction is 76 wt%. The average bulk percentage of smectite in accreted mudstones is 24 wt%, and the highest bulk value is 42 wt% (Fig. F7). We did not complete any additional analyses to pinpoint the type of smectite, but coeval deposits at Site 1177 contain a dioctahedral variety, either montmorillonite or beidellite (**Steurer and Underwood,** this volume). Using the "saddle/peak" method of Rettke (1981), we estimate that the expandability of the smectite at Site 1178 ranges from 55% to 83% (mean = 68%). Therefore, the expandable clay is probably detrital in origin with small amounts of interlayered illite.

DISCUSSION

Potential Sediment Sources

One of the challenges of studying the Nankai margin is to reconstruct patterns of sediment dispersal and account for changes in sediment sources and transport routes through time. The onland geology of central and southwest Japan is composed largely of Mesozoic and early Cenozoic accretionary complexes (Taira et al., 1989; Isozaki et al., 1990). The Inner Zone, which is located on the backarc side of the Median Tectonic Line (Fig. F8), contains low-pressure, high-temperature metamorphic rocks of the Ryoke belt and related granitic rocks (Nakajima, 1997). The Outer Zone consists of parallel bands of high-pressure metamorphic rocks and low-grade meta-sedimentary strata: the Sanbagawa, Chichibu, and Shimanto belts (Taira et al., 1988; Toriumi and Teruya, 1988; Higashino, 1990). Those belts also crop out around the syntaxis structure associated with the collision zone of central Japan (Fig. F8) (Toriumi and Arai, 1989; Kimura, 1996; Takahashi and Saito, 1997). Mechanical weathering of rocks in the Outer Zone should produce a clay mineral assemblage enriched in detrital illite and chlorite with modest amounts of smectite.

We believe that the most noteworthy result from our investigation is the documented change in clay mineralogy from an illite-chlorite assemblage toward a more smectite-rich assemblage at ~3.0 Ma. Smectite group minerals are key tracers for interpretations of clay provenance (e.g., Fagel et al., 2001). Some varieties of smectite form through hydrothermal and/or submarine alteration of basalt and volcanic ash (Chamley, 1989), but the most common origins are meteoric weathering and pedogenesis of volcanic-rich substrates. In general, temporal changes in the abundance of smectite are symptomatic of fluctuations in volcanic eruptions in a fixed source or shifting provenance from volcanic-rich to volcanic-poor terranes. Several regions around Japan need to be considered in this context (Uto and Tatsumi, 1996). The Hohi volcanic zone of central Kyushu formed during a late Miocene phase of north–south extension (6–5 Ma), whereas the more widespread linear chain of active calderas and Pleistocene ignimbrites was emplaced after 1.5 Ma (Kamata and Kodama, 1999). The northeast Honshu arc has been erupting nearly continuously since ~6 Ma (Cambray et al., 1995). Central Japan also contains older welded tuffs of middle–late Miocene age (14–4 Ma) (Otofuji et al., 1997; Kitazato, 1997) and associated granodiorite bodies (12–7 Ma) (Saito et al., 1997). The Izu-Bonin island arc represents a third potential source where marine ash layers record four pulses of volcanic activity since the middle Miocene (Cambray et al., 1995). In addition, voluminous amounts of volcanic detritus were transported into

F8. Sources of sedimentary and meta-sedimentary detritus, p. 24.

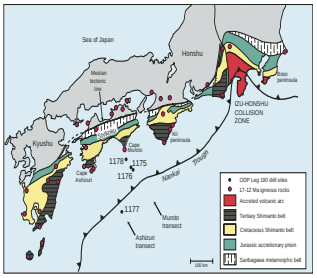

the Shikoku backarc basin by turbidity currents (Hiscott and Gill, 1992; Marsaglia et al., 1995).

Compared to most of Japan, the island of Shikoku and the Kii Peninsula of central Honshu (Fig. F8) are unusual because they are devoid of Holocene volcanic centers. This spatial gap in Quaternary volcanism provides one of the more important constraints on our interpretations of detrital provenance. Quaternary volcanoes exist in southwest Honshu, but they are restricted to the northern side facing the Sea of Japan (Aramaki and Ui, 1977; Uto and Tatsumi, 1996). Weathering of older igneous rocks on Shikoku and Honshu also needs to be considered as a potential source of smectite. Anomalous near-trench silicic magmatism, for example, was widespread in the Outer Zone between 16 and 14 Ma (Fig. F8) (Oba, 1977; Hisatomi, 1988; Terakado et al., 1988; Saito et al., 1997). Coeval Miocene tuffs were recovered offshore at the base of the Shikoku Basin facies (Taira et al., 1992), and onland erosion must have created some volcanic debris from the Outer Zone after magmatism ceased. The Setouchi volcanic belt is slightly younger (13–12 Ma) in age (Tatsumi and Ishizaka, 1982), but the watersheds in that region drain into the interior seaway between Shikoku and Honshu (Fig. F8) rather than into the Philippine Sea. Overall, volcanic rocks are too sparse in the Outer Zone to produce a smectite-rich clay assemblage.

Agents of Suspended Sediment Transport

Reconstruction of ancient sediment dispersal systems is seldom straightforward because suspended sediment in most deep-marine environments is transported by a dynamic combination of surface currents, bottom currents, gravity flows, and biologic resuspension (Gorsline, 1984). In the case of the present-day Nankai margin, the Kuroshio Current generally flows toward the northeast and drives surface water transport off the southeast coast of Kyushu and Shikoku (Fig. F9). Its speed at the surface sometimes exceeds 180 cm/s (Taft, 1972, 1978), although 30–50 cm/s is more typical. The behavior of the Kuroshio Current is complicated. Changes in velocity coincide with the formation and decay of huge meander loops (White and McCreary, 1976; Taira and Teramoto, 1981). The larger meanders seem to be governed by both seafloor morphology (e.g., gaps through the Izu Ridge) and El Niño episodes (Ito and Horikawa, 2000). The warm-water Tsushima Current (Fig. F9) splits off the Kuroshio southwest of Kyushu and drives surface water through the Sea of Japan (Moriyashu, 1972). The cold-water Oyashio Current flows toward the south off northern Japan (Fig. F9). The latitude where Kuroshio–Oyashio convergence occurs shifts over seasonal and glacial–interglacial cycles (Oba and Yasuda, 1992). Thus, over a variety of timescales, surface water circulation changes speed and direction above Nankai Trough and Shikoku Basin.

Documentation of deepwater circulation around Japan remains sketchy. Speeds as high as 40 cm/s have been measured in the Kuroshio deepwater mass at water depths of 2000 m (Ito, 1997), so there is potential for that current to mobilize a near-bottom nepheloid layer over large parts of the Nankai forearc. Taft et al. (1973) showed, however, that mean bottom flow off Kyushu and Shikoku is not in the same direction as the surface flow and is sometimes in the opposite direction. Speeds of 100 cm/s are confined to the upper 500 m of the water column, and nearly all of the northeast-directed transport is restricted to the upper 1000 m (Worthington and Kawai, 1972). Given the water

F9. Sources and transport routes for sediments entering the Nankai subduction margin, p. 25.

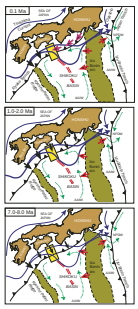

depths of ODP sites in the Muroto Transect (1740–4790 mbsl), the Kuroshio Current has little or no effect on the seafloor.

Another transport agent to consider is thermohaline circulation. Seafloor morphology deflects contour currents around obstructions and funnels water through sills. Contour currents near the Izu Ridge show two directions of motion (Lee and Ogawa, 1998). At depths >2000 m, North Pacific Deep Water flows toward the south-southwest; above 2000 m, flow is toward the north. Because of their hadal depths, the Yap and Mariana Trenches prevent Antarctic Bottom Water (AABW) from entering the Philippine Sea from the Southern Hemisphere, so the north-directed current is probably composed of Antarctic Intermediate Water (AAIW). Exchange of deep bottom water is minimal across the Izu-Bonin Ridge because sill depths are typically 1000–1500 mbsl; instead, AAIW sets up a pattern of counterclockwise rotation around the Shikoku Basin (Lee and Ogawa, 1998). Photographs and direct measurements demonstrate that current speeds in Suruga Trough and eastern Nankai Trough are greater than bedload threshold for fine sand (>20 cm/s) (Okada and Ohta, 1993). The local flow directions are complicated, however, and include both tidal oscillations (up-down canyon axis) and transport toward the northeast (opposite the seafloor gradient of the trench).

Quaternary Dispersal System (<0.46 Ma)

Previous ocean drilling studies showed that late Pleistocene and Holocene turbidites in the modern Nankai trench wedge were derived largely from the collision zone between the Izu-Bonin volcanic arc and Honshu (Fig. **F8**). Those sands contain abundant neovolcanic lithic fragments, sedimentary rock fragments, detrital quartz, and feldspar, and detrital modes are consistent with an undissected to transitional arc provenance (Taira and Niitsuma, 1986; Marsaglia et al., 1992; Underwood et al., 1993; **Fergusson,** this volume). With increasing distance from the Izu-Honshu collision zone, there is gradual enrichment of recycled sedimentary debris and depletion of neovolcanic fragments (Marsaglia et al., 1992). Clay minerals in hemipelagic interbeds of the Nankai trench wedge reflect a more recycled orogen provenance with relatively small amounts of smectite from weathered volcanic sources. Illite is the most abundant clay mineral, followed by chlorite (Chamley et al., 1986; Underwood et al., 1993; **Steurer and Underwood,** this volume). Detailed characteristics of the illite (crystallinity index, mica polytype, and bo values) all point to source areas enriched in low-temperature, low-pressure meta-sedimentary rocks (Underwood et al., 1993). As described previously, terranes that might yield such illite-chlorite clay mineral assemblages are widespread on Shikoku and the Kii Peninsula of Honshu (Fig. **F8**). We suggest, therefore, that the Outer Zone of southwest Japan acted as the principal source of clay entering the late Pleistocene trench. If this interpretation is correct, then the dispersal of suspended sediment (mostly transverse) has been decoupled from the movement of sand (mostly axial flow) (Fig. **F9**).

Downslope movement of turbidity currents to the trench floor is governed primarily by seafloor morphology. At the present time, most through-going conduits (Shiono-misaki Canyon, Tenryu Canyon, and Suruga Trough) are concentrated near the eastern end of Nankai Trough. The suspended sediment budget, on the other hand, is influenced by a combination of surface currents, bottom currents, and gravity flows. Clays are, no doubt, transported along with sand from the

Izu-Honshu collision zone, but that detritus is mixed with and diluted by suspended sediment from a recycled sedimentary source. The Kuroshio Current is the most likely agent for transporting clay in the surface water from Kyushu and western Shikoku into the Muroto segment of the subduction margin (Fig. F9). Another possibility is transverse delivery from southeastern Shikoku by unconfined gravity flows. The ability of muddy turbidity currents to bypass bathymetric obstructions across the forearc should be enhanced with increases in flow thickness and decreases in flow density (e.g., Muck and Underwood, 1990). We suggest that contributions from several sources homogenize in the near-bottom nepheloid layer before settling permanently from suspension.

Late Pliocene–Early Pleistocene Dispersal System (2.0–0.46 Ma)

The late Pliocene was an important episode in the geologic evolution of southwest Japan because it coincided with a shift in the convergence direction of the Philippine Sea plate, counterclockwise rotation in southwest Kyushu, and initiation of pyroclastic volcanism along a well-developed linear chain (Kamata and Kodama, 1999). That tectonic reorganization, however, had little effect on the composition of suspended sediment in the central Nankai forearc. In fact, data from Sites 1175 and 1176 show that the composition of suspended sediment has not changed in a meaningful way during the past 2.0 m.y. We find the same illite-chlorite assemblage throughout the entire slope-basin succession, as well as in the underlying upper Pliocene accretionary prism (Fig. F6). Late Pliocene sand from the accretionary prism, in contrast, is depleted in volcanic debris and enriched in quartz, chert, and sedimentary rock fragments (**Fergusson,** this volume). Our favored explanation for this compositional shift, relative to the axial-flow system of the modern trench, is to funnel most of the sand through canyons and channels that headed along the southern margin of Shikoku (Shipboard Scientific Party, 2001c; Underwood et al., 2003; **Fergusson,** this volume) (Fig. F9).

Several factors probably contributed to the dominance of transverse sediment delivery to the trench and dampening or elimination of axial flow during the late Pliocene. Collision between the Izu-Bonin arc and Honshu began sometime after the middle Miocene opening of the Sea of Japan (Kimura, 1996; Otofuji, 1996), and there have been four discrete stages of collision since that time (Amano, 1991; Takahashi and Saito, 1997). Strata now exposed in the collision zone accumulated between episodes of accretion in deep- to shallow-marine environments (Ogawa et al., 1985; Soh et al., 1991; Kitazato, 1997). Some of that sediment was cannibalized from the collision zone and trapped in nearby subsiding basins (Ito, 1994; Soh et al., 1998). The Japan Alps create the highest relief of central Honshu, but that topography did not form until ~1.2 Ma following east–west collision between the Asian and North American plates (Jolivet et al., 1994). Rapid and widespread uplift, combined with the tectonically driven incision of Suruga Trough, probably redirected the source of Nankai Trough turbidites from Shikoku to the collision zone sometime after 1 Ma.

Several high-resolution studies of sedimentation and paleoceanography have been completed in the Kazusa group, which is a forearc–basin succession that crops out on the north side of the Izu-Honshu collision zone (Boso Peninsula). Those data are important for our interpretations because they provide insights into the behavior of surface currents, bot-

tom currents, and gravity flows between 2.4 and 0.45 Ma. High-frequency depositional sequences in the Kazusa group have been correlated successfully with glacioeustatic cycles using oxygen isotope curves (Ito and Katsura, 1992; Pickering et al., 1999). Paleocurrent directions in sandy contourite facies are highly variable (mostly toward the south-southwest and north-northwest); coeval turbidity currents evidently moved down a northeast-inclined slope and produced a more consistent paleoflow pattern (Ito, 1996). For the most part, paleowater depths were <1000 m (Ito, 1997). Ito (1996, 1997) attributed the Kazusa contourite facies to a deep basal part of the paleo-Kuroshio Current. If his interpretation is correct, then a strong Kuroshio Current also would have transported suspended sediment into the central Nankai forearc from Kyushu and Shikoku (Fig. F9).

Late Miocene–Late Pliocene Dispersal System (9.6–2.0 Ma)

The age at the base of the slope apron at Site 1178 is ~7.2 Ma, and the underlying accretionary prism is 6.8–9.63 Ma. Compared to sands from Sites 1175 and 1176, samples from Site 1178 are depleted in quartz + chert and enriched in sedimentary rock fragments (**Fergusson,** this volume). An immature recycled orogen source in the Outer Zone seems likely. At the same time, the clay budget in the forearc and the trench shifted to a mixture that contained substantially more smectite than what was deposited by the Quaternary system. Some smectite in the slope apron could have been derived from the Hohi volcanic zone of Kyushu, which was active between 6 and 5 Ma (Kamata and Kodama, 1999). A more expansive source, however, was the Izu-Bonin arc, which supplied a smectite-dominated clay assemblage to its forearc throughout the Miocene and Pliocene (Heling et al., 1992). Similar clay assemblages also entered the Shikoku Basin on the backarc side of the volcanic provenance during the same periods of time (Fig. F9) (Chamley, 1980).

As an older geologic relative of the Kazusa group, exposures of the Miura group (14–3 Ma) on the Miura and Boso Peninsulas (Fig. F8) provide a detailed record of volcaniclastic sedimentation prior to collision-induced accretion (Ogawa and Taniguchi, 1988; Soh et al., 1991; Stow et al., 1998). Transport into the Izu forearc basin by turbidity currents was mostly toward the east, whereas paleoflow indicators in contourites show more variation from the southeast to northwest (Stow et al., 1998; Lee and Ogawa, 1998). Because the paleowater depth was 1000–1500 m (or more) during the initial phase of Miura sedimentation, surface currents were probably incapable of transporting sand on the substrate. Instead, the contourites were molded by strong thermohaline circulation. Lee and Ogawa (1998) showed that the bottom currents strengthened at ~6 Ma, a time that may be related to the buildup of ice in Antarctica and intensification of AABW flow (Stow and Faugeres, 1990). On the other hand, the Kuroshio Current and the entire North Pacific subtropical gyre were weaker than they are today because the Central America Seaway remained open (Molina-Cruz, 1997; Tsuchi, 1997).

We suggest that the balance between northeast-directed transport by the Kuroshio Current and transport into the Izu-Bonin backarc by thermohaline and turbidity currents shifted at ~3 Ma (Fig. F9). A weaker Kuroshio Current prior to 3 Ma would have allowed more volcanic sediment into Shikoku Basin and Nankai Trough. Intensification of the Kuroshio Current after 3 Ma increased the supply of illite and chlorite

to the Muroto segment of the Nankai margin at the expense of detrital smectite from the Izu-Bonin arc. It is worth noting that clay mineral assemblages in the Sea of Japan during the same time interval also incorporated more illite and chlorite at the expense of detrital smectite (Fagel et al., 1992). That change has been attributed to strengthening of the Tsushima Current at the end of the Pliocene, which carried more continental sediment from the East China Sea through the Korea Strait into the backarc basin.

CONCLUSIONS

Sources of sediment entering the Nankai-Shikoku subduction zone over the past 10 m.y. have included the Izu-Bonin arc, the Izu-Honshu collision zone, and the Outer Zone of Kyushu, Shikoku, and Honshu. For the most part, the dispersal paths for suspended sediment have been decoupled from transport by turbidity currents. Assemblages of clay minerals from Sites 1175 and 1176 can be used to interpret the provenance of suspended sediment from 2 Ma through the Holocene. The slope-basin succession and underlying accretionary prism at those two sites tapped detrital sources enriched in illite and chlorite, similar to the modern Nankai trench wedge. Smectite contents are typically 25–30 wt% of the clay fraction. A stronger Kuroshio Current should increase the supply of clay from the Outer Zone and dilute the influx of smectite from the Izu-Bonin volcanoes. In comparison, clay assemblages from the slope apron and prism at Site 1178 contain substantially higher percentages of smectite (up to 76 wt% of the clay fraction), particularly in strata older than 3 Ma. We attribute this enrichment of smectite during the early Pliocene and late Miocene to a weaker Kuroshio Current, thereby shifting the balance among detrital inputs toward the Izu-Bonin volcanic source.

ACKNOWLEDGMENTS

We thank Captain Tom Ribbens and the crew, technicians, and fellow scientists aboard *JOIDES Resolution* for their dedicated assistance during Leg 190. This research used samples provided by the Ocean Drilling Program (ODP). ODP is sponsored by the U.S. National Science Foundation and participating countries under management of Joint Oceanographic Institutions, Inc. Funding was provided by the U.S. Science Support Program (grant F001281 to M.B. Underwood) and a Schlanger Ocean Drilling Fellowship to J.A. Steurer. Arpit Ghoting, Anup Bidesi, Nandini Basu, Swati Udas, Marcie Workman, and Eric Grabowski assisted in the laboratory. Martine Buatier and Juichiro Ashi provided helpful reviews of the manuscript. We also thank Greg Moore, Wonn Soh, and Chris Fergusson for insightful discussions regarding regional sediment dispersal.

REFERENCES

Amano, K., 1991. Multiple collision tectonics of the South Fossa Magna in central Japan. *Mod. Geol.,* 15:315–329.

Aramaki, S., and Ui, T., 1977. Major element frequency distribution of the Japanese Quaternary volcanic rocks. *Bull. Volcanol.,* 41:390–407.

Ashi, J., and Taira, A., 1992. Structure of the Nankai accretionary prism as revealed from IZANAGI sidescan imagery and multichannel seismic reflection profiling. *Isl. Arc,* 1:104–115.

Biscaye, P.E., 1965. Mineralogy and sedimentation of Recent deep-sea clays in the Atlantic Ocean and adjacent seas and oceans. *Geol. Soc. Am. Bull.,* 76:803–831.

Blum, P., and Okamura, Y., 1992. Pre-Holocene sediment dispersal systems and effects of structural controls and Holocene sea-level rise from acoustic facies analysis; SW Japan forearc. *Mar. Geol.*, 108:295–322.

Cambray, H., Pubellier, M., Jolivet, L., and Pouclet, A., 1995. Volcanic activity recorded in deep-sea sediments and the geodynamic evolution of western Pacific island arcs. *In* Taylor, B., and Natland, J. (Eds.), *Active Margins and Marginal Basins of the Western Pacific*. Geophys. Monogr., 88:97–124.

Chamley, H., 1980. Clay sedimentation and paleoenvironment in the Shikoku Basin since the middle Miocene (Deep Sea Drilling Project Leg 58, North Philippine Sea). *In* Klein, G.deV., Kobayashi, K., et al., *Init. Repts. DSDP,* 58: Washington (U.S. Govt. Printing Office), 669–678.

————, 1989. *Clay Sedimentology:* Berlin (Springer-Verlag).

Chamley, H., Cadet, J.-P., and Charvet, J., 1986. Nankai Trough and Japan Trench late Cenozoic paleoenvironments deduced from clay mineralogic data. *In* Kagami, H., Karig, D.E., Coulbourn, W.T., et al., *Init. Repts. DSDP,* 87: Washington (U.S. Govt. Printing Office), 633–641.

Coulbourn, W.T., 1986. Sedimentologic summary, Nankai Trough Sites 582 and 583, and Japan Trench Site 584. *In* Kagami, H., Karig, D.E., Coulbourn, W.T., et al., *Init. Repts. DSDP,* 87: Washington (U.S. Govt. Printing Office), 909–926.

Fagel, N., Andre, L., Chamley, H., Debrabant, P., and Jolivet, L., 1992. Clay sedimentation in the Sea of Japan since the early Miocene: influence of source-rock and hydrothermal activity. *Sediment. Geol.,* 80:27–40.

Fagel, N., Robert, C., Preda, M., and Thorez, J., 2001. Smectite composition as a tracer of deep circulation: the case of the northern North Atlantic. *Mar. Geol.,* 172:309–330.

Fisher, A.T., and Underwood, M.B., 1995. Calibration of an X-ray diffraction method to determine relative mineral abundances in bulk powders using matrix singular value decomposition: a test from the Barbados accretionary complex. *In* Shipley, T.H., Ogawa, Y., Blum, P., et al., *Proc. ODP, Init. Repts.,* 156: College Station, TX (Ocean Drilling Program), 29–37.

Gorsline, D.S., 1984. A review of fine-grained sediment origins, characteristics, transport, and deposition. *In* Stow, D.A.V., and Piper, D.J.W. (Eds.), *Fine-Grained Sediments*. Geol. Soc. Spec. Publ., 15:17–34.

Heling, D., Schwarz, A., and Garbe-Schönberg, 1992. X-ray mineralogy and geochemical studies of sediments, Leg 125 Sites 781 through 784 and 786. *In* Fryer, P., Pearce, J.A., Stokking, L.B., et al., *Proc. ODP, Sci. Results,* 125: College Station, TX (Ocean Drilling Program), 115–130.

Higashino, T., 1990. The higher grade metamorphic zonation of the Sambagawa metamorphic belt in central Shikoku, Japan. *J. Metamorph. Geol.,* 8:413–423.

Hiscott, R.N., and Gill, J.B., 1992. Major and trace element geochemistry of Oligocene to Quaternary volcaniclastic sands and sandstones from the Izu-Bonin arc. *In* Taylor, B., Fujioka, K., et al., *Proc. ODP, Sci. Results,* 126: College Station, TX (Ocean Drilling Program), 467–485.

Hisatomi, K., 1988. The Miocene forearc basin of southwest Japan and the Kumano Group of the Kii Peninsula. *Mod. Geol.,* 12:389–408.

Isozaki, Y., Maruyama, S., and Furuoka, F., 1990. Accreted oceanic materials in Japan. *Tectonophysics,* 181:179–205.

Ito, M., 1994. Compositional variation in depositional sequences of the upper part of the Kazusa Group, a middle Pleistocene forearc basin fill in the Boso Peninsula, Japan. *Sediment. Geol.,* 88:219–230.

————, 1996. Sandy contourites of the lower Kazusa Group in the Boso Peninsula, Japan: Kuroshio-Current-influenced deep-sea sedimentation in a Plio-Pleistocene forearc basin. *J. Sediment. Res., Sect. A,* 66:587–598.

————, 1997. Spatial variation in turbidite-to-contourite continuums of the Kiwada and Otadai Formations in the Boso Peninsula, Japan: an unstable bottom-current system in a Plio-Pleistocene forearc basin. *J. Sediment. Res., Sect. A,* 67:571–582.

Ito, M., and Horikawa, K., 2000. Millennial- to decadal-scale fluctuation in the paleo-Kuroshio Current documented in the middle Pleistocene shelf succession on the Boso Peninsula, Japan. *Sediment. Geol.,* 137:1–8.

Ito, M., and Katsura, Y., 1992. Inferred glacio-eustatic control for high-frequency depositional sequences of the Plio-Pleistocene Kazusa Group, a forearc basin fill in Boso Peninsula, Japan. *Sediment. Geol.*, 80:67–75.

Itoh,Y., and Nagasaki, Y., 1996. Crustal shortening of southwest Japan in the late Miocene. *Isl. Arc,* 5:337–353.

Jolivet, L., Tamaki, K., and Fournier, M., 1994. Japan Sea, opening history and mechanism: a synthesis. *J. Geophys. Res.,* 99:22237–22259.

Kamata, H., and Kodama, K., 1999. Volcanic history and tectonics of the southwest Japan arc. *Isl. Arc,* 8:393–403.

Kimura, G., 1996. Collision orogeny at arc-arc junctions in the Japanese Islands. *Isl. Arc.,* 5:262–275.

Kitazato, H., 1997. Paleogeographic changes in central Honshu, Japan, during the late Cenozoic in relation to the collision of the Izu-Ogasawara arc with the Honshu arc. *Isl. Arc,* 6:144–157.

Lee, I.T., and Ogawa, Y., 1998. Bottom-current deposits in the Miocene–Pliocene Misaki Formation, Izu forearc area, Japan. *Isl. Arc,* 7:315–329.

Le Pichon, X., Iiyama, T., Chamley, H., Charvet, J., Faure, M., Fujimoto, H., Furuta, T., Ida, Y., Kagami, H., Lallemant, S., Leggett, J., Murata, A., Okada, H., Rangin, C., Renard, V., Taira, A., and Tokuyama, H., 1987. Nankai Trough and the fossil Shikoku Ridge: results of Box 6 *Kaiko* survey. *Earth Planet. Sci. Lett.,* 83:186–198.

————, 1987. The eastern and western ends of Nankai Trough: results of Box 5 and Box 7 *Kaiko* survey. *Earth Planet. Sci. Lett.,* 83:199–213.

Marsaglia, K.M., Boggs, S., Jr., Clift, P.D., Seyedolali, A., and Smith, R., 1995. Sedimentation in western Pacific backarc basins: new insights from recent ODP drilling. *In* Taylor, B., and Natland, J. (Eds.), *Active Margins and Marginal Basins of the Western Pacific*. Geophys. Monogr., 88:291–314.

Marsaglia, K.M., Ingersoll, R.V., and Packer, B.M., 1992. Tectonic evolution of the Japanese Islands as reflected in modal compositions of Cenozoic forearc and backarc sand and sandstone. *Tectonics,* 11:1028–1044.

Molina-Cruz, A., 1997. Closing of the Central American Gateway and its effects on the distribution of late Pliocene radiolarians in the eastern tropical Pacific. *Tectonophysics,* 281:105–111.

Moore, G.F., and Karig, D.E., 1976a. Development of sedimentary basins on the lower trench slope. *Geology,* 4:693–697.

Moore, G.F., Karig, D.E., Shipley, T.H., Taira, A., Stoffa, P.L., and Wood, W.T., 1991. Structural framework of the ODP Leg 131 area, Nankai Trough. *In* Taira, A., Hill, I., Firth, J.V., et al., *Proc. ODP, Init. Repts.,* 131: College Station, TX (Ocean Drilling Program), 15–20.

Moore, G.F., Taira, A., Bangs, N.L., Kuramoto, S., Shipley, T.H., Alex, C.M., Gulick, S.S., Hills, D.J., Ike, T., Ito, S., Leslie, S.C., McCutcheon, A.J., Mochizuki, K., Morita,

S., Nakamura, Y., Park, J.-O., Taylor, B.L., Yagi, H., and Zhao, Z., 2001a. Data report: Structural setting of the Leg 190 Muroto Transect. *In* Moore, G.F., Taira, A., Klaus, A., et al., *Proc. ODP, Init. Repts.,* 190 [CD-ROM]. Available from: Ocean Drilling Program, Texas A&M University, College Station TX 77845-9547, USA.

Moore, G.F., Taira, A., Klaus, A., and Leg 190 Scientific Party, 2001b. New insights into deformation and fluid flow processes in the Nankai Trough accretionary prism: Results of Ocean Drilling Program Leg 190. *Geochem. Geophys. Geosyst.,* 2:10.1029/2001GC000166.

Moore, J.C., and Karig, D.E., 1976b. Sedimentology, structural geology, and tectonics of the Shikoku subduction zone, southwestern Japan. *Geol. Soc. Am. Bull.,* 87:1259–1268.

Morgan, J.K., Karig, D.E., and Maniatty, A., 1994. The estimation of diffuse strains in the toe of the western Nankai accretionary prism: a kinematic solution. *J. Geophys. Res.,* 99:7019–7032.

Moriyasu, S., 1972. The Tsushima Current. *In* Stommel, H., and Yoshida, K. (Eds.), *Kuroshio, Physical Aspects of the Japan Current:* Seattle (Univ. Washington Press), 353–370.

Muck, M.T., and Underwood, M.B., 1990. Upslope flow of turbidity currents: a comparison among field observations, theory, and laboratory models. *Geology,* 18:54–57.

Nakajima, T., 1997. Regional metamorphic belts of the Japanese Islands. *Isl. Arc,* 6:69–90.

Nakamura, K., Renard, V., Angelier, J., Azema, J., Bourgois, J., Deplus, C., Fujioka, K., Hamano, Y., Huchon, P., Kinoshita, H., Labaume, P., Ogawa, Y., Seno, T., Takeuchi, A., Tanahashi, M., Uchiyama, A., and Vigneresse, J.-L., 1987. Oblique and near collision subduction, Sagami and Suruga Troughs—preliminary results of the French-Japanese 1984 *Kaiko* cruise, Leg 2. *Earth Planet. Sci. Lett.,* 83:229–242.

Oba, N., 1977. Emplacement of granitic rocks in the Outer Zone of southwest Japan and geological significance. *J. Geol.,* 85:383–393.

Oba, T., and Yasuda, H., 1992. Paleoenvironmental change of the Kuroshio region since the last glacial age. *Quat. Res.,* 31:329–339.

Ogawa, Y., Horiuchi, K., Taniguchi, H., and Naka, J., 1985. Collision of the Izu arc with Honshu and the effects of oblique subduction in the Miura-Boso Peninsulas. *Tectonophysics,* 119:349–379.

Ogawa, Y., and Taniguchi, H., 1988. Geology and tectonics of the Miura-Boso Peninsulas and the adjacent area. *Mod. Geol.,* 12:147–168.

Okada, H., and Ohta, S., 1993. Photographic evidence of variable bottom-current activity in the Suruga and Sagami Bays, central Japan. *Sediment. Geol.,* 82:221–237.

Okino, K., and Kato, Y., 1995. Geomorphological study on a clastic accretionary prism: the Nankai Trough. *Isl. Arc,* 4:182–198.

Otofuji, Y.-I., 1996. Large tectonic movement of the Japan arc in late Cenozoic times inferred from paleomagnetism: review and synthesis. *Isl. Arc,* 5:229–249.

Otofuji, Y-I., Nishizawa, Y., Tamai, M., and Matsuda, T., 1997. Palaeomagnetic and chronological study of Miocene welded tuffs in the northern part of central Japan: tectonic implications for the latest stage of arc formation of Japan. *Tectonophysics,* 283:263–278.

Pickering, K.T., Souter, C., Oba, T., Taira, A., Schaaf, M., and Platzman, E., 1999. Glacio-eustatic control on deep-marine clastic forearc sedimentation, Pliocene–mid-Pleistocene (c. 1180–600 ka) Kazusa Group, SE Japan. *J. Geol. Soc. (London, U.K.),* 156:125–136.

Rettke, R.C., 1981. Probable burial diagenetic and provenance effects on Dakota Group clay mineralogy, Denver Basin. *J. Sediment. Petrol.,* 51:541–551.

Saito, K., Kato, K., and Sugi, S., 1997. K-Ar dating studies of Ashigawa and Tokuwa granodiorite bodies and plutonic geochronology in the South Fossa Magna, central Japan. *Isl. Arc,* 6:158–167.

Scholl, D.W., von Huene, R., Vallier, T.L., and Howell, D.G., 1980. Sedimentary masses and concepts about tectonic processes at underthrust ocean margins. *Geology,* 8:564–568.

Shimamura, K., 1989. Topography and sedimentary facies of the Nankai deep sea channel. *In* Taira, A., and Masuda, F. (Eds.), *Sedimentary Facies in the Active Plate Margin:* Tokyo (Terra Sci. Publ.), 529–556.

Shipboard Scientific Party, 2001a. Explanatory notes. *In* Moore, G.F., Taira, A., Klaus, A., et al., *Proc. ODP, Init. Repts.,* 190, 1–51 [CD-ROM]. Available from: Ocean Drilling Program, Texas A&M University, College Station TX 77845-9547, USA.

————, 2001b. Leg 190 summary. *In* Moore, G.F., Taira, A., Klaus, A., et al., *Proc. ODP, Init. Repts.,* 190: College Station TX (Ocean Drilling Program), 1–87.

————, 2001c. Site 1175. *In* Moore, G.F., Taira, A., Klaus, A., et al., *Proc. ODP, Init. Repts.,* 190, 1–92 [CD-ROM]. Available from: Ocean Drilling Program, Texas A&M University, College Station TX 77845-9547, USA.

————, 2001d. Site 1176. *In* Moore, G.F., Taira, A., Klaus, A., et al., *Proc. ODP, Init. Repts.,* 190, 1–80 [CD-ROM]. Available from: Ocean Drilling Program, Texas A&M University, College Station TX 77845-9547, USA.

————, 2001e. Site 1178. *In* Moore, G.F., Taira, A., Klaus, A., et al., *Proc. ODP, Init. Repts.,* 190, 1–108 [CD-ROM]. Available from: Ocean Drilling Program, Texas A&M University, College Station TX 77845-9547, USA.

Soh, W., Nakayama, K., and Kimura, T., 1998. Arc-arc collision in the Izu collision zone, central Japan, deduced from the Ashigara Basin and adjacent Tanzawa Mountains. *Isl. Arc,* 7:330–341.

Soh, W., Pickering, K.T., Taira, A., and Tokuyama, H., 1991. Basin evolution in the arc-arc Izu collision zone, Mio-Pliocene Miura Group, central Japan. *J. Geol. Soc. (London, U.K.),* 148:317–330.

Soh, W., Tanaka, T., and Taira, A., 1995. Geomorphology and sedimentary processes of a modern slope-type fan delta (Fujikawa fan delta), Suruga Trough, Japan. *Sediment. Geol.,* 98:79–95.

Stow, D.A.V., and Faugeres, J.C., 1990. Miocene contourites from the proto Izu-Bonin forearc region, southern Japan. *Int. Sedimentol. Congr.,* 13:526. (Abstract)

Stow, D.A.V., Taira, A., Ogawa, Y., Soh, W., Taniguchi, H., and Pickering, K.T., 1998. Volcaniclastic sediments, process interaction and depositional setting of the Mio-Pliocene Miura Group, SE Japan. *Sediment. Geol.,* 115:351–381.

Taft, B.A., 1972. Characteristics of the flow of the Kuroshio south of Japan. *In* Stommel, H., and Yoshida, K. (Eds.), *Kuroshio: Physical Aspects of the Japan Current:* Seattle (Univ. Washington Press), 165–216.

————, 1978. Structure of the Kuroshio south of Japan. *J. Mar. Res.,* 16:77–117.

Taft, B.A., Robinson, A.R., and Schmitz, W.J., 1973. Current path and bottom velocity of the Kuroshio. *J. Phys. Oceanogr.,* 3:347–350.

Taira, A., and Ashi, J., 1993. Sedimentary facies evolution of the Nankai forearc and its implications for the growth of the Shimanto accretionary prism. *In* Hill, I.A., Taira, A., Firth, J.V., et al., *Proc. ODP, Sci. Results,* 131: College Station, TX (Ocean Drilling Program), 331–341.

Taira, A., Hill, I., Firth, J., Berner, U., Brückmann, W., Byrne, T., Chabernaud, T., Fisher, A., Foucher, J.-P., Gamo, T., Gieskes, J., Hyndman, R., Karig, D., Kastner, M., Kato, Y., Lallement, S., Lu, R., Maltman, A., Moore, G., Moran, K., Olaffson, G., Owens, W., Pickering, K., Siena, F., Taylor, E., Underwood, M., Wilkinson, C., Yamano, M., and Zhang, J., 1992. Sediment deformation and hydrogeology of the Nankai accretionary prism: synthesis of shipboard results of ODP Leg 131. *Earth Planet. Sci. Lett.,* 109:431–450.

Taira, A., Katto, J., Tashiro, M., Okamura, M., and Kodama, K., 1988. The Shimanto Belt in Shikoku, Japan: evolution of Cretaceous to Miocene accretionary prism. *Mod. Geol.,* 12:5–46.

Taira, A., and Niitsuma, N., 1986. Turbidite sedimentation in the Nankai Trough as interpreted from magnetic fabric, grain size, and detrital modal analyses. *In* Kag-

ami, H., Karig, D.E., Coulbourn, W.T., et al., *Init. Repts. DSDP,* 87: Washington (U.S. Govt. Printing Office), 611–632.

Taira, A., Tokuyama, H., and Soh, W., 1989. Accretion tectonics and evolution of Japan. *In* Ben-Avraham, Z. (Ed.), *The Evolution of Pacific Ocean Margins:* Oxford (Oxford Univ. Press), 100–123.

Taira, K., and Teramoto, T., 1981. Velocity fluctuations of the Kuroshio near the Izu Ridge and their relationship to current path. *Deep-Sea Res.,* 28A:1187–1197.

Takahashi, M., and Saito, K., 1997. Miocene intra-arc bending at the arc-arc collision zone, central Japan. *Isl. Arc,* 6:168–182.

Tatsumi, Y., 1982. Origin of high-magnesian andesites in the Setouchi volcanic belt, southwest Japan. II. Melting phase relations at high pressures. *Earth Planet. Sci. Lett.,* 60:305–317.

Terakado, Y., Shimizu, H., and Masuda, A., 1988. Nd and Sr isotopic variations in acidic rocks formed under a peculiar tectonic environment in Miocene southwest Japan. *Contrib. Mineral. Petrol.,* 99:1–10.

Toriumi, M., and Arai, T., 1989. Metamorphism of the Izu-Tanzawa collision zone. *Tectonophysics,* 160:293–303.

Toriumi, M., and Teruya, J., 1988. Tectono-metamorphism of the Shimanto Belt. *Mod. Geol.,* 12:303–324.

Tsuchi, R., 1997. Marine climatic responses to Neogene tectonics of the Pacific Ocean seaways. *Tectonophysics,* 281:113–124.

Underwood, M.B., and Bachman, S.G., 1982. Sedimentary facies associations within subduction complexes. *In* Leggett, J.K. (Ed.), *Trench-Forearc Geology: Sedimentation and Tectonics on Modern and Ancient Active Plate Margins*. Geol. Soc. Spec. Publ., 10:537–550.

Underwood, M.B., and Moore, G.F., 1995. Trenches and trench-slope basins. *In* Busby, C., and Ingersoll, R.V. (Eds.), *Tectonics of Sedimentary Basins*: Cambridge, MA (Blackwell Science), 179-219.

Underwood, M.B., Moore, G.F., Taira, A., Klaus, A., Wilson, M.E.J., Fergusson, C.L., Hirano, S., Steurer, J., and Leg 190 Shipboard Scientific Party, 2003. Sedimentary and tectonic evolution of a trench-slope basin in the Nankai subduction zone of southwest Japan. *J. Sediment. Res.*, 73:589–602.

Underwood, M.B., Orr, R., Pickering, K., and Taira, A., 1993. Provenance and dispersal patterns of sediments in the turbidite wedge of Nankai Trough. *In* Hill, I.A., Taira, A., Firth, J.V., et al., *Proc. ODP, Sci. Results,* 131: College Station, TX (Ocean Drilling Program), 15–34.

Uto, K., and Tatsumi, Y., 1996. Quaternary volcanism of the Japanese Islands. *Isl. Arc,* 5:250–261.

White, W.B., and McCreary, J.P., 1976. On the formation of the Kuroshio meander and its relationship to the large-scale ocean circulation. *Deep-Sea Res.,* 23:33–47.

Worthington, L.V., and Kawai, H., 1972. Comparison between deep sections across the Kuroshio and the Florida Current and the Gulf Stream. *In* Stommel, H., and Yoshida, K. (Eds.), *Kuroshio: Physical Aspects of the Japan Current:* Seattle (Univ. Washington Press), 371–386.

Figure F1. Bathymetric map of Nankai Trough and the northern edge of Shikoku Basin. Numbers refer to sites of the Deep Sea Drilling Project and the Ocean Drilling Program. Bathymetry is in meters. Modified from Shipboard Scientific Party (2001b).

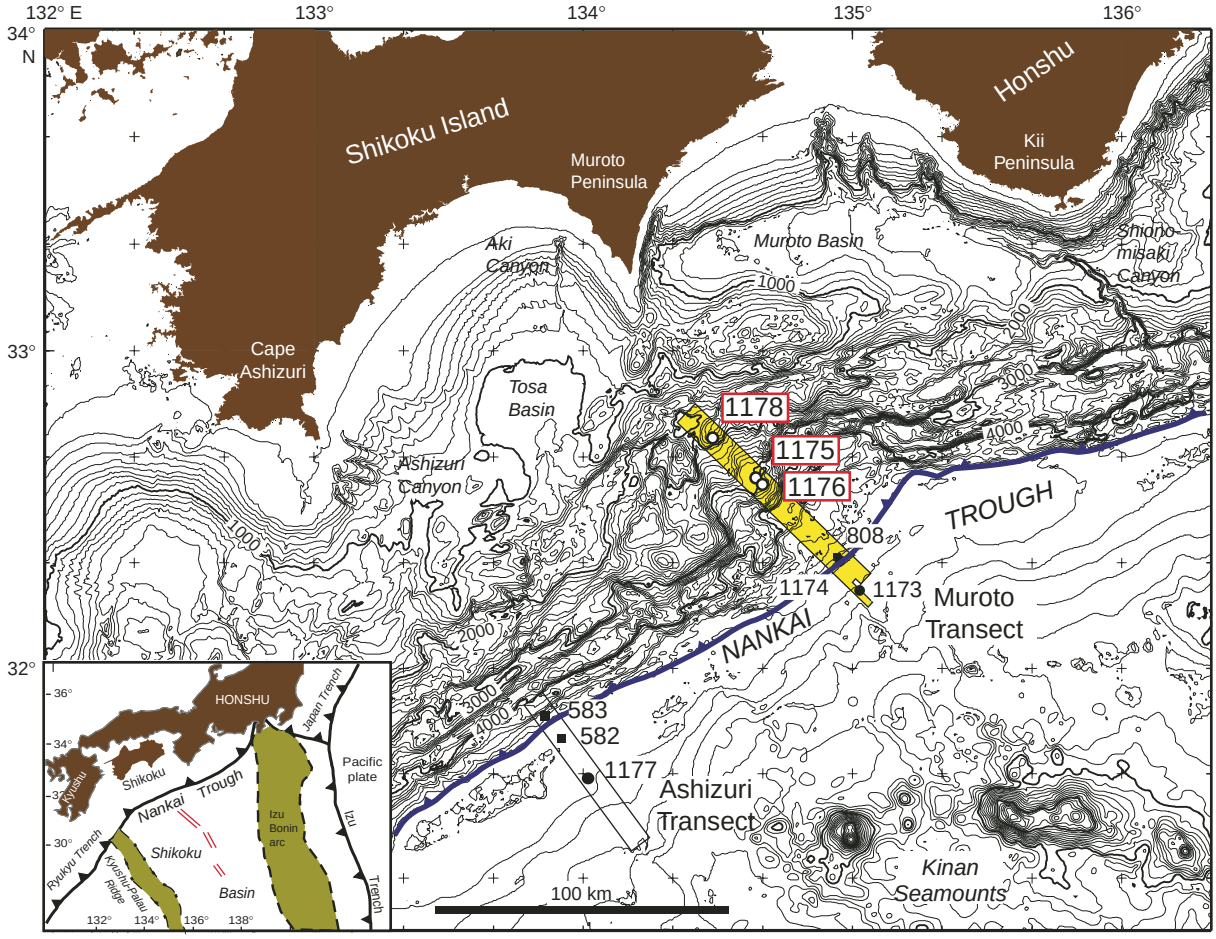

Figure F2. Interpretive cross section of the Nankai accretionary prism showing four zones of seismic reflection structure in the Muroto Transect area (modified from Shipboard Scientific Party 2001b). Numbers refer to ODP drill sites. V.E. = vertical exaggeration.

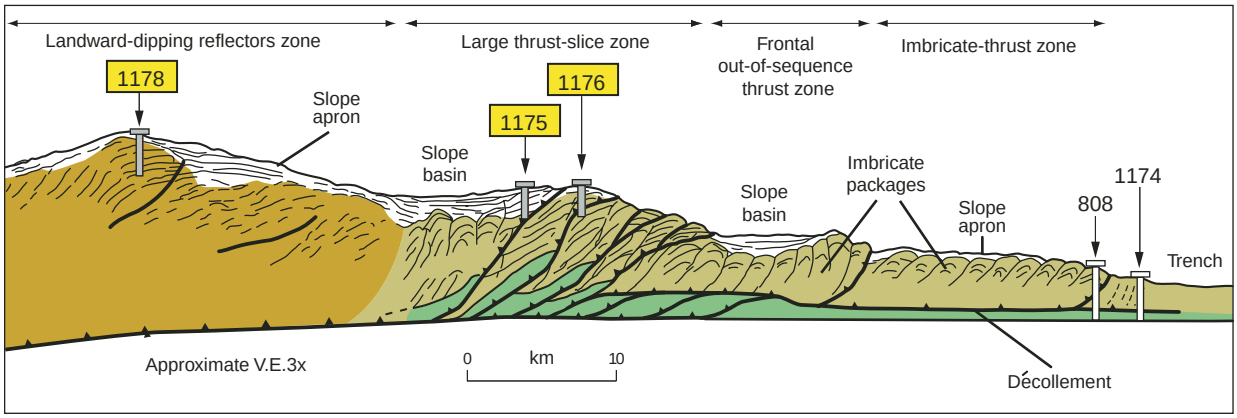

Figure F3. Lithostratigraphic and biostratigraphic correlation for Sites 1175, 1176, and 1178 of the Nankai forearc. Stratigraphic ages (in Ma) are from Shipboard Scientific Party (2001c, 2001d, 2001e) and Boeckel (pers. comm., 2003).

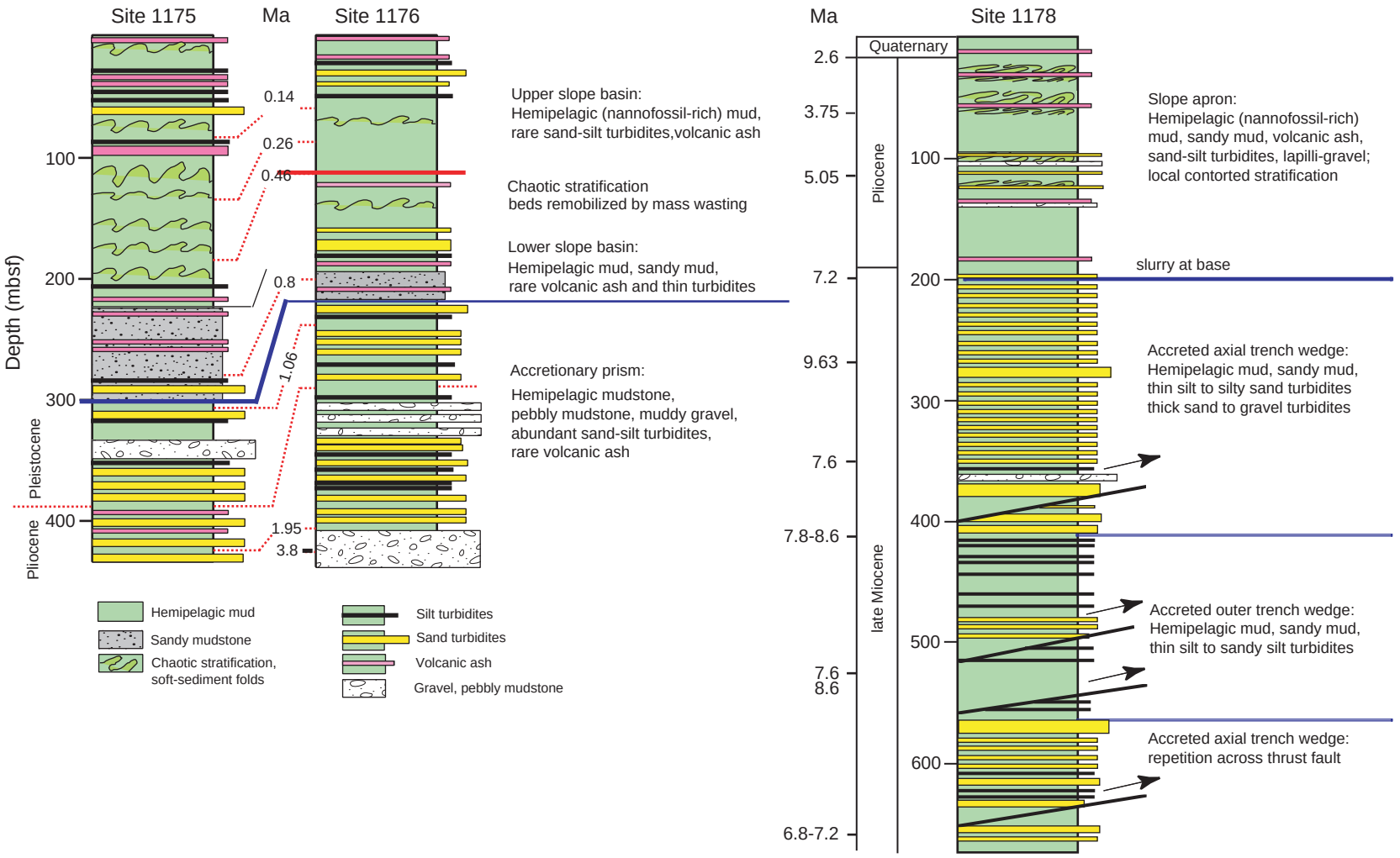

Figure F4. Representative examples of X-ray diffractograms showing peaks for smectite, illite, chlorite, kaolinite, and quartz. Values of relative mineral abundance (wt%) in oriented aggregates of the <2-µm size fraction are based on SVD normalization factors (**Underwood et al.,** this volume) and the following peaks: smectite (001), illite (001), chlorite (002) + kaolinite (001), and quartz (100).

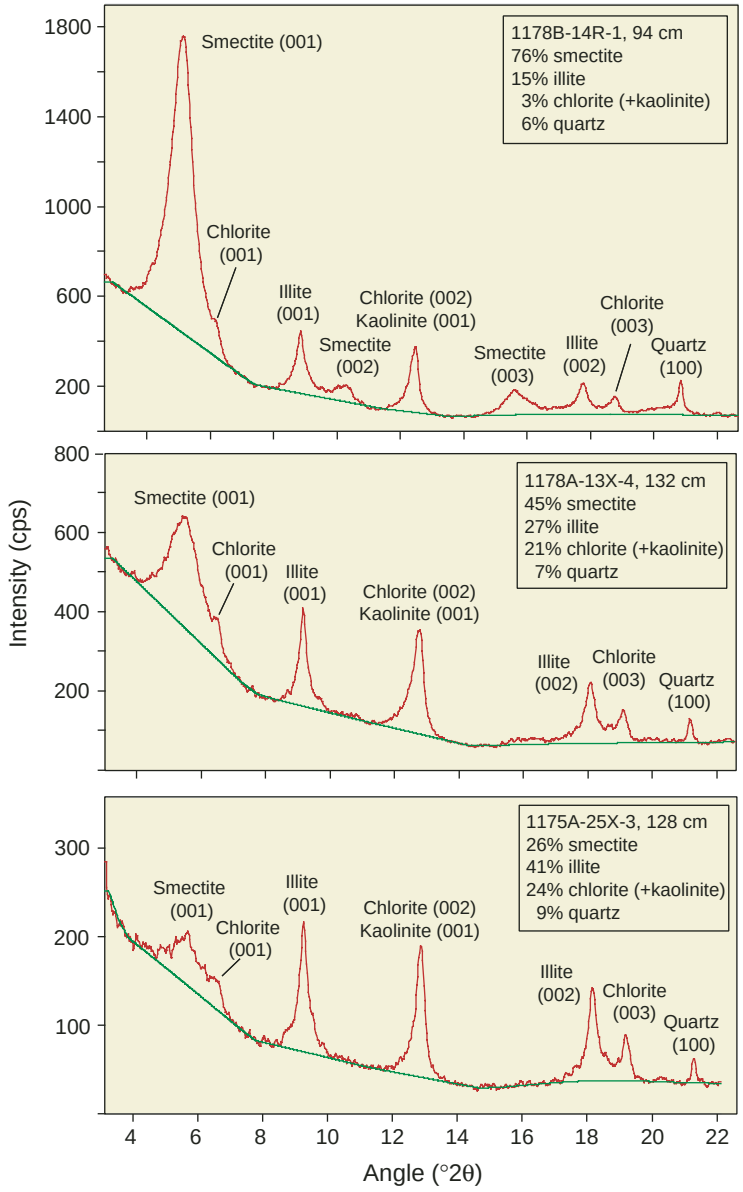

Figure F5. Relative abundance of calcite and total clay minerals in bulk samples from Sites 1175, 1176, and 1178, Nankai forearc. Values of relative mineral abundance (wt%) are based on X-ray diffraction analysis of random bulk powders (Shipboard Scientific Party 2001c, 2001d, 2001e).

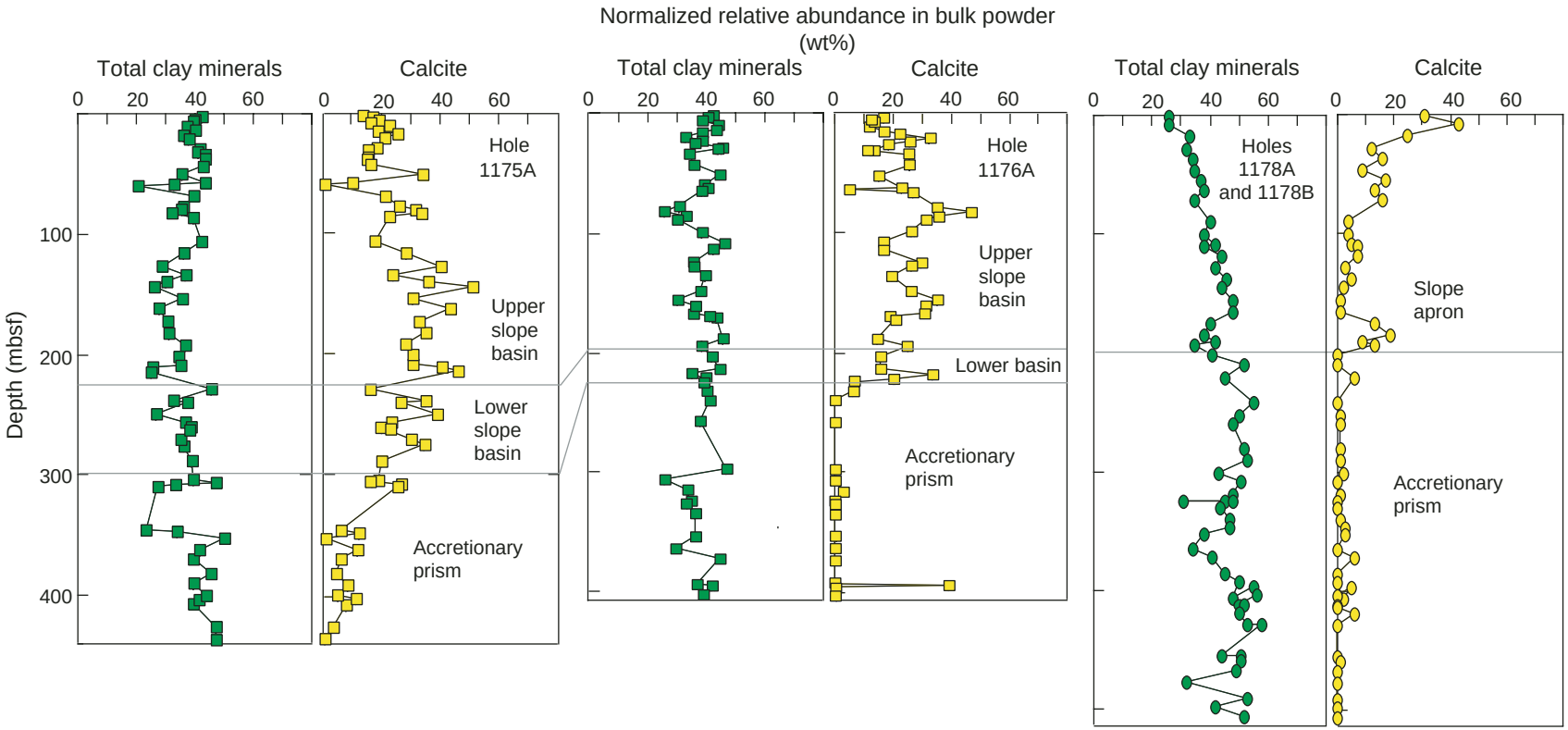

Figure F6. Relative abundance of smectite, illite, chlorite (+ kaolinite), and quartz in mud and mudstone from Sites 1175 and 1176. Solid symbols = values (wt%) in the <2-µm size fraction. Open symbols = calculated values (wt%) for each clay mineral in bulk samples.

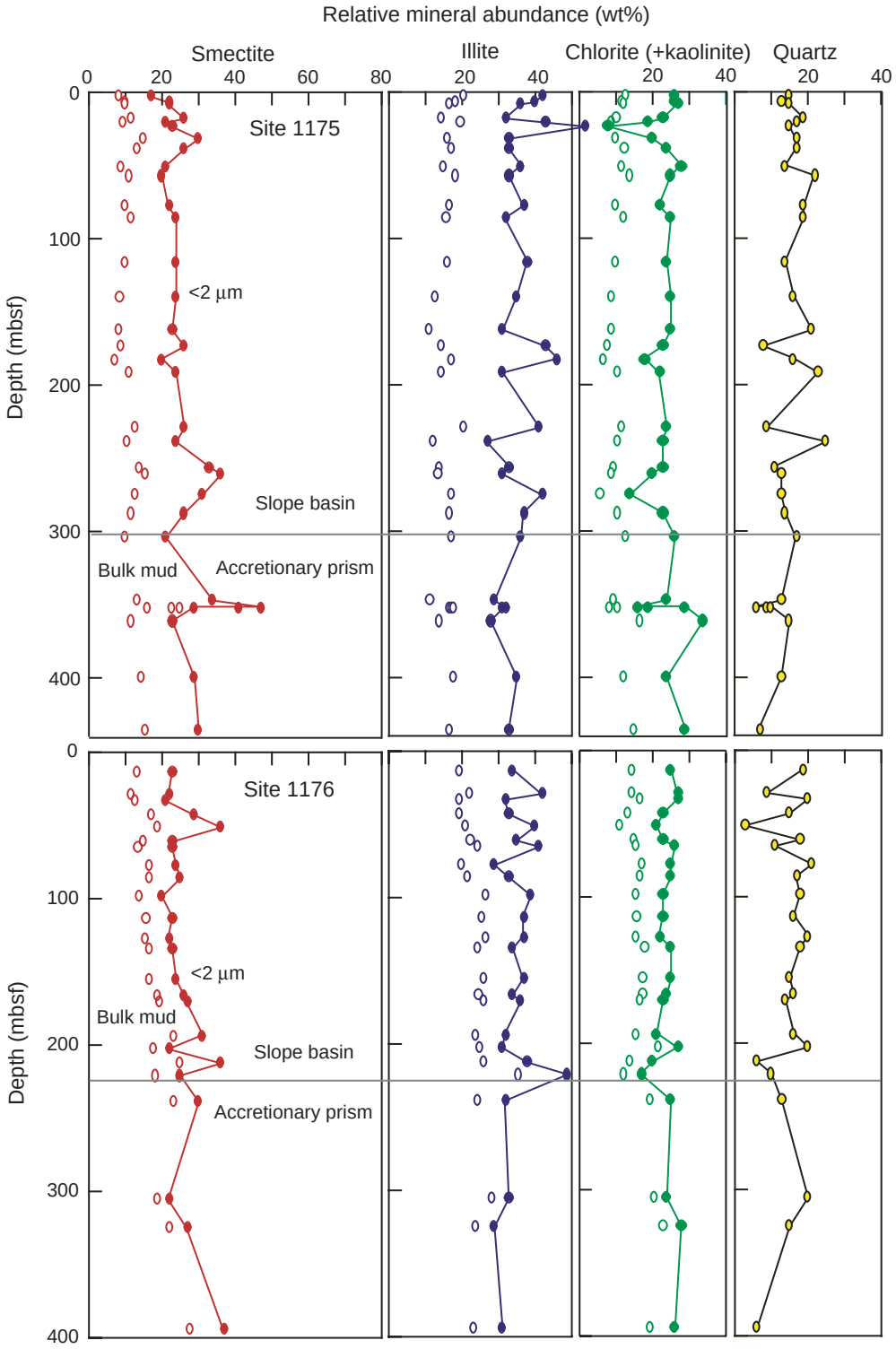

Figure F7. Relative abundance of smectite, illite, chlorite (+ kaolinite), and quartz in mud and mudstone from Site 1178. Solid symbols = values (wt%) in the <2-µm size fraction. Open symbols = calculated values (wt%) for each clay mineral in bulk samples.

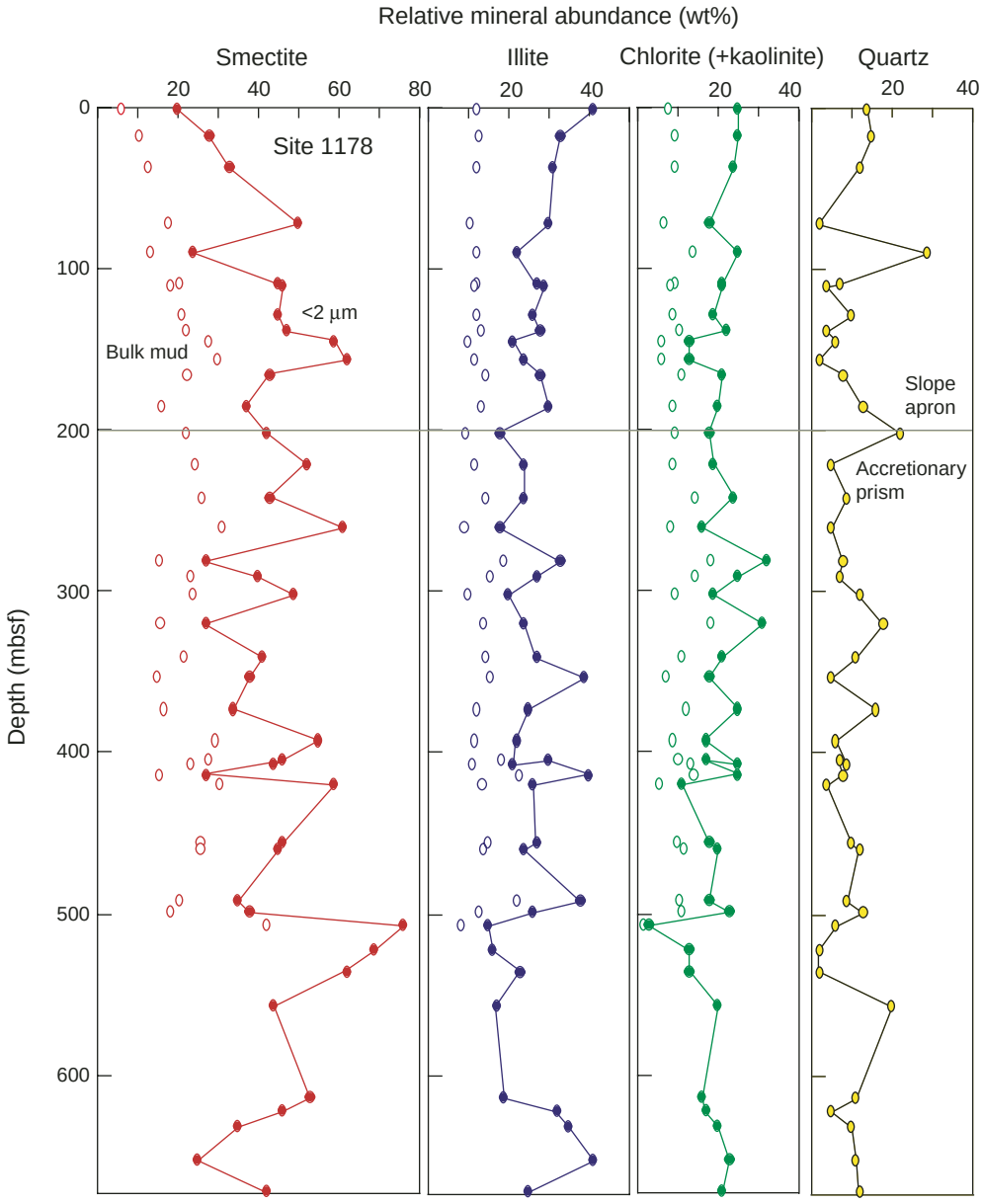

Figure F8. Simplified geologic map showing principal sources of sedimentary and metasedimentary detritus entering the Nankai Trough and forearc from the Outer Zone of southwest Japan. The Izu-Honshu collision zone at the northeast edge of Nankai Trough also contains neovolcanic source rocks. Numbers refer to ODP sites. Modified from Shipboard Scientific Party (2001b).

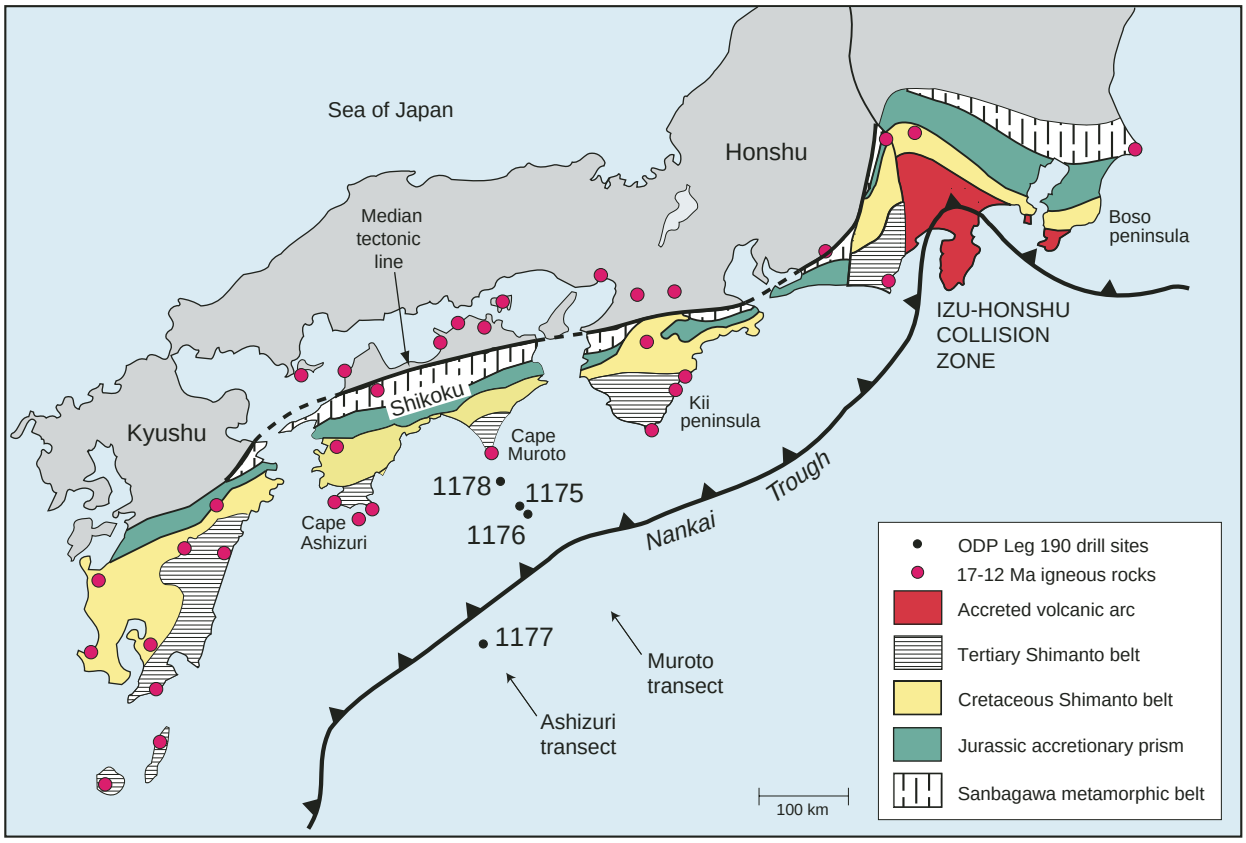

Figure F9. Schematic illustrations of sources and transport routes for sediments entering the Nankai subduction margin during three intervals of time: late Quaternary (0.1 Ma), late Pliocene–early Pleistocene (1.0–2.0 Ma), and late Miocene (7.0–8.0 Ma). Yellow box = location of study area. Surface currents are shown in solid blue; meander in Kuroshio Current is generalized from White and McCreary (1976). Bottom currents are shown in dashed green: AAIW = Antarctic Intermediate Water; NPDW = North Pacific Deep Water. Bold arrows depict transport directions for turbidity currents and other gravity flows: red = Izu-Bonin arc source; purple = Izu-Honshu collision zone source; black = Outer Zone source.

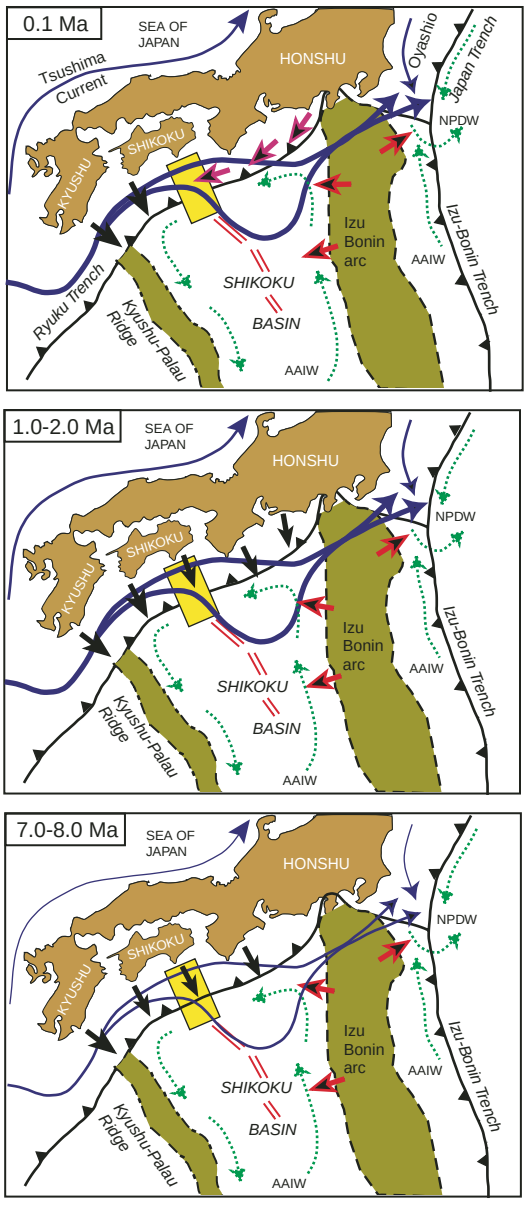

Table T1. Results of X-ray diffraction analyses, oriented clay aggregates, trench-slope site. (**See table notes.** Continued on next two pages.)

Core, section, interval (cm)	Depth (mbsf)	<2-μm fraction: XRD peak area (total counts)				<2-μm fraction: SVD factor (wt%)				Clay minerals only: SVD factor (wt%)			Clay minerals only: Biscaye (area%)			Bulk mudstone: SVD factor (wt%)			
		Smectite	Illite	Chlorite*	Quartz	Smectite	Illite	Chlorite	Quartz	Smectite	Illite	Chlorite	Smectite	Illite	Chlorite	Total clay	Smectite	Illite	Chlorite
190-1175A-																			
1H-2, 137	2.87	913	3,808	3,810	388	17	42	26	15	20	49	31	4	64	32	42	8	21	13
1H-5, 67	6.67	2,474	3,505	3,743	341	22	40	26	13	25	45	30	10	58	31	40	10	18	12
2H-1, 134	8.54	1,576	1,956	2,483	268	22	36	27	15	26	42	32	11	54	35	39	10	17	12
3H-1, 137	18.07	1,927	1,775	2,007	395	26	32	23	19	32	40	28	15	54	31	36	12	14	10
3H-3, 137	21.07	1,128	3,052	2,012	391	21	43	19	17	25	52	23	6	70	23	38	10	20	9
3H-5, 127	23.97	1,828	5,812	1,581	506	23	54	8	15	27	64	9	6	82	11	NA			
4H-4, 139	32.09	4,161	2,834	2,837	545	30	33	20	17	36	40	24	20	54	27	41	15	16	10
5H-2, 134	38.54	2,427	2,223	2,585	411	26	33	24	17	31	40	29	15	54	31	43	13	17	12
6H-4, 108	50.78	1,829	2,413	3,100	310	21	36	28	14	25	42	33	10	55	35	35	9	15	12
7H-2, 129	57.49	1,128	3,117	3,625	765	20	33	25	22	26	42	32	5	60	35	43	11	18	14
9H-3, 129	77.99	942	1,735	1,547	310	22	37	22	19	27	46	27	9	63	28	36	10	16	10
10H-2, 135	86.05	2,009	2,168	2,796	477	24	32	25	19	30	40	31	12	53	34	40	12	16	12
13H-4, 131	116.11	1,768	2,103	2,229	255	24	38	24	14	28	44	28	12	57	30	36	10	16	10
16H-1, 73	139.53	2,748	2,895	3,485	457	24	35	25	16	29	42	30	13	54	33	30	9	13	9
18H-3, 140	162.20	1,256	1,575	2,012	428	23	31	25	21	29	39	32	11	54	35	28	8	11	9
19H-4, 125	173.15	6,136	6,236	5,901	383	26	43	23	8	28	47	25	14	58	28	31	9	14	8
20H-4, 137	182.67	783	2,949	1,823	330	20	46	18	16	24	55	21	5	73	22	31	7	17	7
21H-4, 131	192.11	1,543	2,047	2,214	591	24	31	22	23	31	40	29	11	58	31	36	11	14	10
25X-3, 128	228.88	7,391	6,474	6,599	460	26	41	24	9	29	45	26	16	56	28	45	13	20	12
26X-3, 125	238.55	1,093	1,348	1,776	549	24	27	23	25	32	36	31	11	54	35	33	11	12	10
28X-2, 119	256.29	5,774	3,005	3,646	396	33	33	23	11	37	37	26	23	48	29	37	14	14	10
28X-5, 113	260.73	7,631	3,329	3,864	539	36	31	20	13	41	36	23	27	46	27	38	16	14	9
30X-2, 111	275.41	3,770	3,290	1,928	387	31	42	14	13	36	48	16	18	63	19	36	13	17	6
31X-4, 117	288.07	4,723	4,440	4,525	553	26	37	23	14	30	43	27	15	56	29	39	12	17	10
			Average slope-basin facies:			25	37	22	16								11	16	10
33X-2, 116	304.26	1,892	2,890	3,486	458	21	36	26	17	25	43	31	9	57	34	40	10	17	13
37X-5, 136	347.36	9,425	3,885	5,714	681	34	29	24	13	39	33	28	26	43	31	34	13	11	9
38X-2, 116	352.26	26,378	8,031	8,509	872	47	31	16	6	50	33	17	35	43	23	50	25	16	9
38X-2, 116	352.26	16,880	5,917	6,740	807	41	31	19	9	45	34	21	31	44	25	50	23	17	10
38X-2, 116	352.26	9,752	5,559	8,645	605	29	32	29	10	32	36	32	20	45	35	50	16	18	16
39X-2, 100	361.70	4,033	2,891	6,459	565	23	28	34	15	27	33	40	14	41	45	42	11	14	17
43X-2, 67	399.77	7,589	5,195	6,132	688	29	35	24	13	33	40	27	19	51	30	44	15	18	12
47X-CC, 11	435.51	9,684	5,186	8,082	399	30	33	29	7	33	36	32	21	45	35	47	15	17	15
			Average accretionary prism:			32	32	25	11								16	16	13
190-1176A-																			
2H-4, 136	13.26	2,138	2,691	3,150	537	23	34	25	19	28	41	30	11	56	33	47	13	19	14
4H-2, 138	29.28	2,576	3,220	3,559	199	22	42	27	9	24	46	30	11	57	32	48	12	22	14
4H-5, 134	33.74	879	1,377	1,831	306	21	32	27	20	26	40	34	9	55	36	49	13	20	17
5H-5, 72	42.62	3,709	2,577	3,066	416	29	33	23	15	34	39	27	18	51	30	50	17	19	14
6H-4, 104	50.94	5,410	2,893	2,940	115	36	40	21	3	37	41	22	24	51	26	51	19	21	11
7H-4, 124	60.64	1,958	2,704	2,796	488	23	35	23	18	28	43	28	11	59	30	52	15	22	15
8H-1, 74	65.14	3,918	4,691	4,982	370	23	41	26	11	26	46	29	12	57	31	53	14	24	15
9H-3, 128	78.18	1,447	1,468	2,081	416	24	29	25	21	31	37	32	13	51	36	54	17	20	17
10H-2, 80	85.70	1,832	1,794	2,192	331	25	33	25	17	30	40	30	14	54	33	55	17	22	17
11H-4, 108	98.48	1,012	2,690	2,487	420	20	39	23	18	24	48	28	6	64	30	56	14	27	16
13H-1, 128	113.18	2,715	3,661	3,666	539	23	37	23	16	28	45	28	11	59	30	57	16	25	16

Table T1 (continued).

Core, section, interval (cm)	Depth (mbsf)	<2-µm fraction: XRD peak area (total counts)				<2-µm fraction: SVD factor (wt%)				Clay minerals only: SVD factor (wt%)			Clay minerals only: Biscaye (area%)			Bulk mudstone: SVD factor (wt%)			
		Smectite	Illite	Chlorite*	Quartz	Smectite	Illite	Chlorite	Quartz	Smectite	Illite	Chlorite	Smectite	Illite	Chlorite	Total clay	Smectite	Illite	Chlorite
14H-4, 132	127.22	1,173	2,637	2,360	496	22	37	22	20	27	46	27	7	64	29	58	16	26	16
15H-3, 131	135.21	1,589	2,242	2,635	434	23	34	25	18	28	41	30	10	57	33	59	17	24	18
17H-4, 131	155.71	2,770	3,068	3,457	417	24	37	25	15	28	43	29	13	56	31	60	17	26	17
19H-3, 126	166.66	3,453	3,043	3,459	500	26	34	24	16	31	40	29	15	54	31	61	19	25	17
20X-1, 40	171.00	3,454	3,008	3,146	403	27	36	23	14	31	42	27	16	55	29	62	19	26	17
22X-3, 102	193.92	4,040	2,495	2,668	463	31	32	21	16	37	38	25	21	52	28	63	23	24	16
23X-3, 63	203.13	1,370	1,942	2,713	481	22	31	27	20	28	39	34	9	53	37	64	18	25	22
24X-3, 84	212.94	14,127	7,327	7,488	479	36	38	20	6	38	40	21	24	50	26	65	25	26	14
25X-2, 123	221.43	4,490	6,563	4,074	433	25	49	17	10	27	54	19	12	68	21	66	18	36	12
				Average slope-basin facies:		25	36	24	15	29	42	28					17	24	16
27X-1, 122	239.12	8,469	4,721	6,478	689	30	32	25	13	34	37	29	21	47	32	67	23	25	19
34X-CC, 20	305.50	2,287	3,541	4,141	807	22	33	24	20	28	42	30	9	57	33	68	19	28	21
36X-1, 26	324.76	4,496	2,777	4,657	530	27	29	28	15	32	35	33	18	45	37	69	22	24	23
43X-2, 125	394.75	18,796	7,020	10,922	561	37	31	26	6	39	33	28	27	41	32	70	28	23	19
				Average accretionary prism:		29	31	26	14								23	25	21
190-1178A-																			
1H-1, 133	1.33	1,596	3,026	3,070	326	20	41	25	14	23	48	29	8	61	31	26	6	12	8
3H-4, 133	18.23	3,869	2,798	3,578	457	28	33	25	15	33	38	29	17	50	32	33	11	13	10
5H-4, 138	37.28	8,691	4,089	5,603	608	33	31	24	12	38	35	27	24	45	31	34	13	12	9
9X-5, 129	72.03	40,810	10,976	13,571	713	50	30	18	2	51	31	18	36	39	24	35	18	11	6
11X-4, 124	90.54	1,113	1,345	2,723	961	24	22	25	29	34	31	35	9	45	46	40	14	12	14
13X-4, 132	109.82	35,535	9,727	14,351	1,184	45	27	21	7	48	29	23	34	38	28	42	20	12	9
13X-5, 123	111.23	38,010	10,825	15,030	869	46	29	21	4	48	30	22	34	39	27	38	18	11	8
15X-4, 130	129.00	44,575	11,713	15,844	2,041	45	26	19	10	50	29	21	36	38	26	42	21	12	9
16X-4, 128	138.48	52,464	13,837	20,622	1,170	47	28	22	4	48	29	23	35	37	28	46	22	13	10
17X-2, 125	144.95	96,563	15,685	21,233	2,976	59	21	13	6	63	23	14	48	31	21	44	28	10	6
18X-4, 130	156.46	85,360	15,199	19,198	1,650	62	24	13	2	63	24	13	46	33	21	48	30	12	6
19X-3, 125	165.65	41,153	12,073	17,121	1,531	43	28	21	8	47	30	23	33	39	28	48	22	15	11
21X-4, 121	186.11	5,034	2,057	2,388	372	37	30	20	13	43	34	23	28	46	26	38	16	13	9
				Average slope-apron facies:		41	28	21	10								18	12	9
23X-2, 117	201.87	29,422	4,944	9,310	3,461	42	18	18	22	54	23	23	43	29	27	41	22	9	9
25X-2, 118	221.05	56,158	11,222	18,263	1,543	52	24	19	5	55	25	20	41	33	27	45	25	11	9
27X-3, 120	242.00	20,309	4,880	9,048	867	43	24	24	9	47	26	26	35	34	31	55	26	15	15
29X-3, 122	260.93	80,467	10,770	19,033	2,120	61	18	16	5	64	19	17	50	27	24	48	31	9	8
31X-4, 116	281.86	27,330	15,770	27,046	1,314	27	33	32	8	29	36	35	19	44	37	52	15	19	18
32X-4, 120	291.05	8,544	2,537	4,348	310	40	27	25	7	43	29	27	31	37	32	53	23	16	14
33X-5, 118	302.68	25,280	4,318	7,944	1,271	49	20	19	12	56	23	22	43	30	27	43	24	10	9
35X-4, 120	320.50	5,505	2,604	6,313	836	27	24	31	18	33	29	38	19	36	44	48	16	14	18
37X-5, 120	341.20	19,660	5,828	8,361	1,055	41	27	21	11	46	30	24	33	39	28	47	22	14	11
39X-1, 15	353.35	16,399	8,392	7,726	500	38	39	18	5	40	41	19	25	51	24	38	15	16	7
41X-1, 89	373.39	8,146	2,756	5,079	745	34	25	25	16	40	30	30	28	38	35	41	17	12	12
43X-1, 121	392.81	86,308	15,513	24,636	2,473	55	22	17	6	59	23	18	44	31	25	50	29	12	9
44X-5, 117	407.69	24,565	4,830	10,987	1,007	44	21	25	9	49	23	28	37	29	33	48	23	11	13
190-1178B-																			
3R-3, 147	404.47	72,671	21,525	24,925	2,484	46	30	17	7	49	32	18	35	41	24	56	28	18	10
4R-3, 127	413.87	9,999	8,518	9,194	583	27	40	25	8	29	43	27	16	55	29	52	15	23	14

Table T1 (continued).

Core, section, interval (cm)	Depth (mbsf)	XRD peak area (total counts)				<2-μm fraction SVD factor (wt%)				Clay minerals only SVD factor (wt%)			Clay minerals only Biscaye (area%)			Bulk mudstone SVD factor (wt%)			
		Smectite	Illite	Chlorite*	Quartz	Smectite	Illite	Chlorite	Quartz	Smectite	Illite	Chlorite	Smectite	Illite	Chlorite	Total clay	Smectite	Illite	Chlorite
5R-1, 114	420.44	115,683	23,430	25,036	3,039	59	26	11	4	61	27	11	45	36	19	50	31	14	6
8R-6, 67	456.37	31,410	8,368	10,537	1,492	46	27	18	10	51	30	20	37	39	25	51	26	15	10
9R-2, 117	460.47	26,141	6,286	9,634	1,387	45	24	20	12	51	27	22	37	36	27	51	26	14	11
12R-4, 112	492.32	38,726	21,606	19,402	1,930	35	38	18	9	38	42	20	24	53	24	53	20	22	10
13R-2, 80	498.70	38,607	12,245	19,885	2,536	38	26	23	13	44	30	26	30	38	31	42	18	13	11
14R-1, 94	506.94	132,316	12,782	12,835	3,938	76	15	3	6	81	16	3	63	24	12	52	42	8	2
15R-5, 103	522.63	167,191	17,811	33,886	3,273	69	16	13	2	70	16	13	55	23	22	NA			
17R-1, 105	535.85	119,749	20,235	27,285	2,361	62	23	13	2	63	23	13	47	32	21	NA			
19R-2, 144	556.94	26,977	3,785	9,120	2,488	44	17	20	20	54	21	25	45	25	30	NA			
25R-2, 98	614.18	51,052	7,903	13,160	2,371	53	19	16	11	60	22	18	47	29	24	NA			
26R-1, 116	622.56	61,948	20,246	21,724	1,716	46	32	17	5	48	34	18	33	43	23	NA			
27R-1, 98	631.98	25,869	13,324	13,645	1,567	35	35	20	10	39	39	22	24	50	26	NA			
29R-2, 96	652.86	7,182	7,892	7,758	718	25	41	23	11	28	46	26	13	58	29	NA			
31R-2, 136	672.46	21,742	5,998	9,179	1,205	42	25	21	12	48	28	24	34	37	29	NA			
				Average accretionary prism:		45	26	20	9								24	14	11

Notes: * = (+ kaolinite). SVD (singular value decomposition) normalization factors from **Underwood et al.** (this volume). Peak area weighting factors from Biscaye (1965). Total clay minerals in bulk mudstone from Shipboard Scientific Party (2001c, 2001d, 2001e). NA = not analyzed.